The RAG1 Ubiquitin Ligase Domain Enhances the Assembly and Selection of T Cell Receptor Genes to Restrain the Autoimmune Hazard of Generating T Cell Receptor Diversity

Thomas N. Burn*[,†,1]; Charline Miot[‡,1]; Scott M. Gordon*[,§]; Erica J. Culberson[‡]; Tamir Diamond *[,¶]; Portia A. Kreiger[‡]; Katharina E. Hayer[‖]; Anamika Bhattacharyya[#,**], Jessica M. Jones[#], Craig H. Bassing*[,‡,2]; Edward M. Behrens*[,†,2]

*Institute for Immunology, Perelman School of Medicine, University of Pennsylvania, Philadelphia, PA 19104
[†]Division of Rheumatology, The Children's Hospital of Philadelphia, Philadelphia, PA 19104
[‡]Department of Pathology and Laboratory Medicine, The Children's Hospital of Philadelphia, Philadelphia, PA 19104
[§]Division of Neonatology, The Children's Hospital of Philadelphia, Philadelphia, PA 19104
[¶]Division of Gastroenterology, Hepatology, and Nutrition, The Children's Hospital of Philadelphia, Philadelphia, PA 19104
[‖]Department of Biomedical and Health Bioinformatics, The Children's Hospital of Philadelphia, Philadelphia, PA 19104
[#]Department of Biochemistry and Molecular and Cellular Sciences, Georgetown University, Washington, DC, 20057
[**]Present Address: Vyome Therapeutics Lt., 501 Patparganj Industrial Area, Dehli, India
[††]Department of Pathology and Laboratory Medicine, The Perelman School of Medicine of the University of Pennsylvania, Philadelphia, PA 19104

[1]Co-first Authors

[2]Co-corresponding Authors:
Craig H. Bassing, Ph.D.
Children's Hospital of Philadelphia
4054 Colket Translational Research Building
3501 Civic Center Blvd.
Philadelphia, PA 19104
Phone: 267-426-0311
Email: bassing@email.chop.edu

Edward M. Behrens, M.D.
Children's Hospital of Philadelphia
1102 Abramson Research Center
3615 Civic Center Boulevard
Philadelphia, PA 19104
Phone: 267-426-0142
Email: behrens@email.chop.edu

Abstract

RAG1/RAG2 (RAG) endonuclease-mediated assembly of diverse lymphocyte antigen receptor genes by V(D)J recombination is critical for the development and immune function of T and B cells. However, this process creates highly self-reactive cells that must be properly selected to suppress autoimmunity. The RAG1 protein contains a ubiquitin ligase domain that stabilizes RAG1 and stimulates RAG endonuclease activity *in vitro*. We report that mice with a mutation that inactivates the RAG1 ubiquitin ligase *in vitro* exhibit modestly reduced thymic cellularity, decreased assembly and altered repertoires of T cell receptor (TCR) β and α genes in thymocytes, and impaired thymocyte developmental transitions that require the assembly of TCRβ or α genes and signaling by their proteins. These RAG1 mutant mice also exhibit less efficient positive selection and superantigen-mediated negative selection of conventional αβ T cells, 2) impaired differentiation of iNKT lineage αβ T cells, and 3) $CD4^+$ αβ T cells with elevated autoimmune potential. Our findings demonstrate that the RAG1 ubiquitin ligase domain functions *in vivo* to stimulate the assembly and selection of TCRβ and TCRα genes, thereby establishing replete diversity of αβ TCRs and αβ T cell lineages while restraining the inherent autoimmune hazard of generating diverse antigen specificities.

Introduction

The ability of T and B lymphocyte populations to express antigen receptors able to recognize a potentially unlimited number of distinct pathogens is the fundamental basis of adaptive immunity. RAG1/RAG2 (RAG) endonuclease-mediated assembly of T cell receptor (TCR) and immunoglobulin (Ig) genes through V(D)J recombination establishes this vast pool of diverse receptors. Germline TCR and Ig loci consist of variable (V), joining (J), and sometimes diversity (D), gene segments residing upstream of constant (C) region exons. During T and B cell development, the lymphocyte-specific RAG complex cooperates with lineage- and developmental stage-specific activation of TCR and Ig loci to perform V(D)J recombination (1). RAG induces DNA double strand breaks (DSBs) adjacent to two participating gene segments and cooperates with DSB repair factors to create V(D)J coding joins that comprise the second exons of assembled V(D)J-C antigen receptor genes (1, 2). The broad utilization of high numbers of gene segments and imprecision in V(D)J coding join formation creating a hypervariable complementatry-determineing region (the CDR3 region) cooperate to produce a vast population of diverse antigen receptor genes. Due to imprecise means of opening and processing coding ends, the outcomes of V(D)J recombination include out-of-frame genes unable to make protein and receptors that recognize self-antigens and have potential for autoimmunity. Accordingly, developing T and B lymphocytes engage quality control checkpoints to select for potentially beneficial antigen receptor proteins and against hazardous highly self-reactive receptors.

Both immature T and B cells employ developmental programs that link functional protein expression from in-frame V(D)J rearrangements to signal either survival and continued differentiation or apoptosis (1). The maturation of αβ T cells in the thymus provides a paradigm for how V(D)J recombination and antigen receptor protein quality control checkpoints cooperate to create a large pool of lymphocytes with diverse receptors that provides immunity from pathogens without causing overt autoimmunity. After entering the

91 thymus, early thymocyte progenitor cells differentiate into $CD44^+CD25^+$ stage 2 and then into $CD44^-$
92 $CD25^+$ stage 3 $CD4^-CD8^-$ double negative (DN) thymocytes (3, 4). Both DN2 and DN3 cells express RAG
93 and conduct V(D)J recombination of *Tcrb*, *Tcrd*, and/or *Tcrg* loci (3, 4). Although DN2-to-DN3
94 thymocyte maturation can occur independent of RAG and V(D)J recombination, an in-frame *Tcrb*
95 rearrangement is necessary for development beyond the DN3 stage (3, 4). The resultant TCRβ protein
96 associates with invariant pTα protein to produce pre-TCR complexes that signal antigen-independent
97 survival, proliferation, and differentiation of DN3 cells (β-selection) into $CD44^-CD25^-$ stage 4 DN
98 thymocytes and then $CD4^+CD8^+$ double-positive (DP) thymocytes (3, 4). DP cells express RAG and
99 conduct V(D)J recombination of *Tcra* loci, which typically proceeds through successive rounds of V-to-J
100 rearrangement on both alleles (5). After an in-frame VJ rearrangement, the resulting TCRα protein can
101 pair with TCRβ protein and yield surface αβ TCRs, which must signal to prevent death by neglect (6-9).
102 This signal activation requires appropriate physical interactions between αβ TCRs and self-peptide/MHC
103 (pMHC) complexes displayed on thymic epithelial cells (TECs) or dendritic cells (DCs), meaning that a
104 functional αβ TCR is inherently self-reactive (6-9). Interactions below a particular low threshold of
105 affinity (or avidity) cannot activate signalling to block apoptosis (6-9). At the other extreme, contacts
106 above a higher threshold trigger strong signals that causes apoptosis (negative selection) to delete highly
107 self-reactive cells with substantial autoimmune potential (6-9). Contacts between these thresholds activate
108 TCR signals of a strength within a range that promotes survival and differentiation of DP cells (positive
109 selection) into $CD4^+$ or $CD8^+$ single-positive (SP) thymocytes, which lack RAG expression and exit the
110 thymus as mature αβ T cells (6-9). Strong TCR signals in DP cells can also activate an alternative agonist
111 selection process that promotes differentiation of unconventional αβ T cell lineages: regulatory T (T reg)
112 cells, intestinal intraepithelial lymphocytes (IELs), and invariant natural killer T (iNKT) cells (6, 7).
113

114 The RAG1 protein N-terminus has a Zinc-binding RING finger ubiquitin ligase domain of undetermined
115 relevance for antigen receptor gene assembly. *In vitro,* RAG1 autoubiquitylates on lysine 233 (10), which
116 enhances RAG endonuclease activity *in vitro* as evidenced by impaired cleavage upon mutation of this
117 residue (11). *In vitro,* RAG1 also ubiquitylates other proteins including histone H3 within chromatin (12,
118 13). RAG1 RING domain mutations that disrupt ubiquitin ligase activity impair RAG-mediated cleavage
119 and joining of chromatin substrates in cell lines, which could be due to loss of histone H3 ubiquitylation
120 and/or alteration in RAG1 protein structure (13-15). The C328Y mutation of a critical structural zinc-
121 binding cysteine of human RAG1 impairs V(D)J recombination and causes severe T and B cell
122 immunodeficiency associated with uncontrolled proliferation of activated oligoclonal αβ T cells (16). The
123 analogous C325Y mutation of mouse Rag1 protein (C325Y) *in vitro* destabilizes Rag1 tertiary structure,
124 abrogates ubiquitin ligase activity, and reduces V(D)J recombination (22). Mice with homozygous Rag1
125 C325Y mutation have a near complete block of αβ T cell development at the DN3 thymocyte stage due
126 to impaired *Tcrb* recombination (14, 15). RING domains have a conserved proline (proline 326 in mouse
127 Rag1) that is critical for ubiquitin ligase activity by permitting functional interaction with ubiquitin-
128 conjugating enzymes (17, 18). Relative to C325Y mutation, P326G mutation abrogates Rag1 ubiquitin
129 ligase activity equivalently, but has substantially less severe effects on both destabilizing tertiary structure
130 of the Rag1 RING domain and reducing RAG endonuclease activity (15). Accordingly, P326 mutation of
131 endogenous mouse Rag1 protein allows an approach to elucidate potential physiologic roles of the RAG1
132 ubiquitin ligase domain beyond promoting V(D)J recombination by stabilizing RAG1 protein structure.
133
134 To determine potential *in vivo* functions of RAG1 ubiquitin ligase activity, we created and analyzed mice
135 carrying a homozygous Rag1 P326G mutation. These mice exhibit phenotypes indicative of lower than
136 normal RAG endonuclease activity including impaired B cell development, elevated Igκ^{+}:Igλ^{+} B cell ratio,
137 and decreased assembly of *Igh*, *Ig*κ, *Ig*λ, and *Tcrb* genes (19). We show here that these mice exhibit

138 decreased levels and altered repertoires of *Tcrb* or *Tcra* rearrangements in DN3 or DP thymocytes,
139 respectively, correlating with lower fractions of each cells selected for further differentiation. We find that
140 the αβ TCR-signaled upregulation of CD69 is diminished during the initiation of positive selection. When
141 assaying αβ TCRs expressing specific TCRβ or TCRα chains, we observe diminished efficiencies for
142 superantigen-mediated negative selection of conventional αβ T cells and differentiation of iNKT lineage
143 αβ T cells. Finally, we show that mature $CD4^+$ effector αβ T cells of these mice exhibit normal immune
144 responses to activation, yet possess greater intrinsic potential for autoimmunity. Our data demonstrate that
145 the RAG1 ubiquitin ligase domain functions *in vivo* to stimulate TCRβ and TCRα gene assembly and
146 αβ TCR selection, thereby generating replete αβ TCR diversity and αβ T cell lineages while restraining
147 the inherent autoimmune hazard of establishing diverse TCR specificities. We discuss how the RAG1
148 ubiquitin ligase domain might function *in vivo* to regulate the assembly of TCRβ and TCRα genes,
149 selection of αβ TCRs, and differentiation of αβ T cell lineages.

150 **Results**

151

152

153 **Homozygous Rag1 P326G mutation diminishes TCR gene assembly and subsequent thymocyte**

154 **developmental stage transitions.**

155 To determine potential *in vivo* functions of the RAG1 ubiquitin ligase, we created and analyzed C57BL/6

156 strain mice homozygous for the Rag1 P326G mutation (*Rag1*$^{P326G/P326G}$ mice; see Materials and Methods)

157 that abrogates RAG1 ubiquitin ligase activity but minimally destabilizes RAG1 protein (15). We initially

158 analyzed αβ T cell development and TCR gene rearrangements in *Rag1*$^{P326G/P326G}$ (*PG*) mice and wild-

159 type (*WT*) mice. As compared to *WT* mice, *PG* mice have a ~2-fold higher percentage and number of DN3

160 thymocytes and correspondingly lower percentage and number of DN4 thymocytes (Fig. 1, A and B). *PG*

161 mice also exhibit ~10% reductions in the percentage and number of DP thymocytes and the ratio of CD4^{+}

162 SP thymocytes to DP thymocytes (Fig. 1, C-E). Despite these minor impairments of the DN3-to-DN4 and

163 DP-to-SP thymocyte developmental transitions, *PG* mice have normal numbers of total thymocytes and

164 splenic αβ T cells (Fig. 1 F). Using Taqman PCR to amplify Vβ rearrangements to Dβ1Jβ1.1, Dβ1Jβ2.1,

165 or Dβ2Jβ2.1 complexes in non-selected DN3 cells, we observed ~50% lower levels of rearrangement for

166 nearly all individual Vβ segments in *PG* mice (Fig. 2, A and B). Notably, the recombination of some Vβ

167 segments involving Jβ2.1 were undetectable in *PG* mice (Fig. 2, A and B), indicating altered Jβ repertoire

168 from Rag1^{P326G} mutation. *Rag1* or *Rag2* mutations that substantially decrease RAG endonuclease activity,

169 thymocyte development, and thymic cellularity, also alter the usage of individual Vβ segments (20, 21).

170 However, high-throughput sequencing of *Tcrb* rearrangements in DN3 thymocytes shows similar usage

171 of each Vβ segment in *PG* and *WT* mice (Fig. 2 C), reflecting the modest reduction of *Tcrb* gene assembly

172 in *PG* mice. This analysis also reveals modest alterations in Dβ and Jβ usage, but no difference in CDR3β

173 lengths in the *Tcrb* rearrangements of *PG* mice (Fig. 2, D and E; data not shown). Using Taqman PCR to

174 amplify a subset of possible Vα-to-Jα rearrangements in non-selected DP thymocytes, we detected lower

175 levels of rearrangements for many of the Vα/Jα combinations, particularly those involving the two most

176 distal Jα gene segments (Jα17, Jα2) tested, in *PG* mice (Fig. 2, F). Together, these data indicate that
177 homozygous Rag1^{P326G} mutation produces RAG endonuclease complexes that catalyze decreased levels
178 of *Tcrb* and *Tcra* rearrangements, alter the primary repertoires of *Tcrb* and *Tcra* genes, and support less
179 efficient thymocyte developmental transitions that depend on the functional assembly of a *Tcrb* or *Tcra*
180 gene. The lower efficiency of overall *Tcrb* and *Tcra* gene assembly certainly contributes to the diminished
181 DN3-to-DP and DP-to-SP thymocyte developmental progressions observed in *PG* mice.
182
183 Notably, the degrees to which TCR gene rearrangements and αβ T cell development are reduced in *PG*
184 mice are dramatically less severe than reported for homozygous Rag1 C235Y mutation (14). For example,
185 Rag1^{P236G} mice generate 90% of the normal number of DP thymocytes, whereas homozygous Rag1^{C235Y}
186 mice produce only 1% of the normal number of DP thymocytes. The markedly different severities of these
187 phenotypes suggest that abrogation of Rag1 ubiquitin ligase activity without substantial disruption of Rag1
188 protein structure only slightly impairs V(D)J recombination and αβ T cell development. Notably, the
189 Rag1^{P326G} protein is expressed at modestly higher levels in thymocytes than wild-type Rag1 protein (19),
190 indicating that reduced Rag1 protein expression levels do not contribute to the slightly impaired
191 development of αβ T cells in *PG* mice. As we were not able to detect Rag1 ubiquitin ligase activity in *WT*
192 mice, we could not confirm the expected abrogation of Rag1 ubiqutin ligase activity in *PG* mice that was
193 observed with Rag1^{P236G} mutation *in vitro*, leaving open the possibility that the mutant Rag1^{P326G} protein
194 exhibits some level of ubiquitin ligase activity *in vivo*.
195
196 To confirm that the impaired development of αβ T cells in PG mice is due to cell intrinsic properties, we
197 made and analyzed competitive bone marrow chimeric mice. These data show no signficiant differences
198 in contributions of *WT* cells and *PG* cells at each of DN thymocyte stages (Supplemental Figure 1A). In
199 marked contrast, there were greater contributions of *WT* cells at the DP and both SP thymocyte stages and

200 within the $CD4^+$ and $CD8^+$ splenic αβ T cell populations (Supplemental Figure 1A, B). The data support

201 the notion that the decreased progression of $Rag1^{P326G}$ thymocytes beyond the DN stage is due to cell

202 intrinsic alterations, most likely from the decreased assembly of TCRβ genes.

203

Figure 1

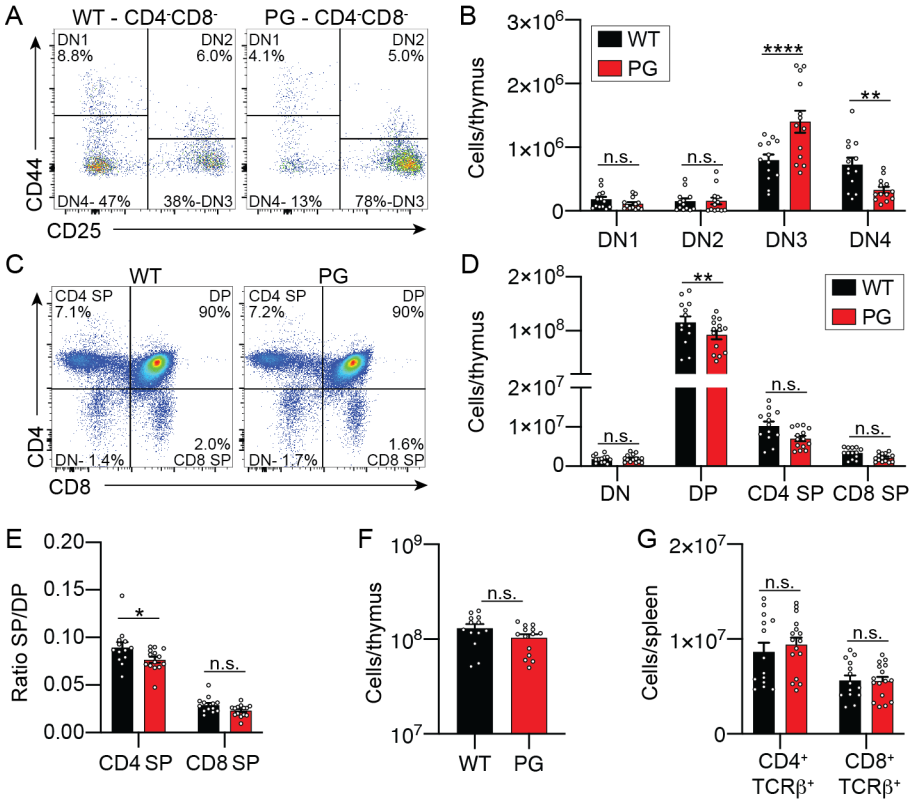

Figure 1. *PG* mice exhibit impaired thymocyte developmental transitions that require TCR gene assembly. **(A)** Representative flow cytometry plots of DN stages of thymocyte development showing the frequency of cells at each stage. **(B)** Quantification of numbers of cells in each DN stage. **(C)** Representative flow cytometry plots of DN, DP, $CD4^+$ SP, and $CD8^+$ SP thymocytes. **(D)** Quantification of numbers of cells in each stage. **(E)** Quantification of the ratio of $CD4^+$ SP or $CD8^+$ SP thymocytes to DP thymocytes. **(F-G)** Quantification of the numbers of total thymocytes (F) and splenic αβ T cells (G). (A-G) All data were collected from 6-10 weeks old mice and (B, D, E, F, and G) are combined from four independent experiments including a total of 14-16 mice per genotype. Bars indicate mean +/- SEM. Stats: 2-way ANOVA with Sidak multiple comparison test. n.s. $p>0.05$; * $p<0.05$, ** $p<0.01$, *** $p<0.001$, **** $p<0.0001$.

Figure 2

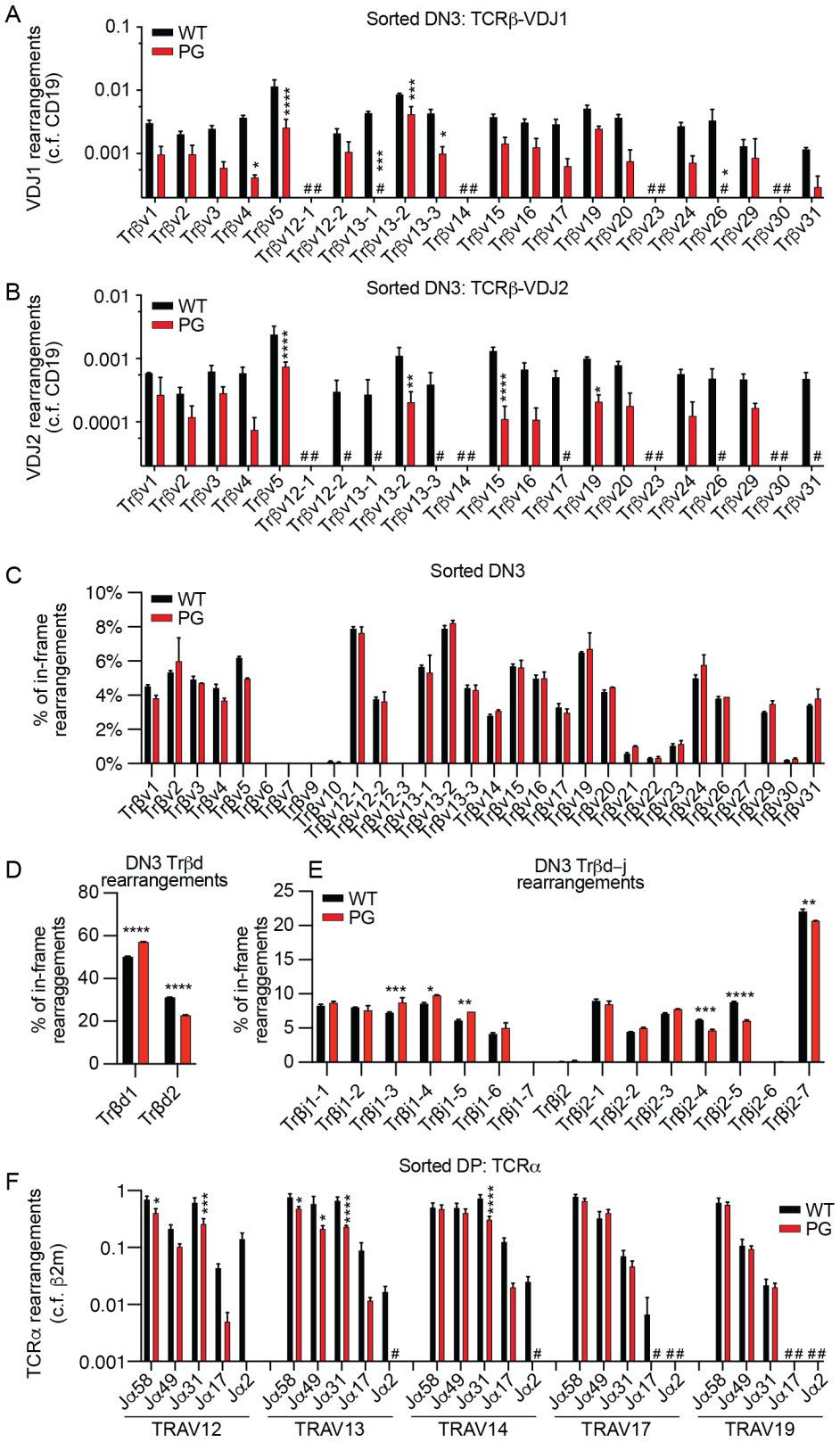
A
Sorted DN3: TCRβ-VDJ1
VDJ1 rearrangements (c.f. CD19)
WT
PG
0.1
0.01
0.001
Trβv1 Trβv2 Trβv3 Trβv4 Trβv5 Trβv12-1 Trβv12-2 Trβv13-1 Trβv13-2 Trβv13-3 Trβv14 Trβv15 Trβv16 Trβv17 Trβv19 Trβv20 Trβv23 Trβv24 Trβv26 Trβv29 Trβv30 Trβv31
B
Sorted DN3: TCRβ-VDJ2
VDJ2 rearrangements (c.f. CD19)
0.01
0.001
0.0001
C
Sorted DN3
% of in-frame rearrangements
10%
8%
6%
4%
2%
0%
Trβv1 Trβv2 Trβv3 Trβv4 Trβv5 Trβv6 Trβv7 Trβv9 Trβv10 Trβv12-1 Trβv12-2 Trβv12-3 Trβv13-1 Trβv13-2 Trβv13-3 Trβv14 Trβv15 Trβv16 Trβv17 Trβv19 Trβv20 Trβv21 Trβv22 Trβv23 Trβv24 Trβv26 Trβv27 Trβv29 Trβv30 Trβv31
D
DN3 Trβd rearrangements
% of in-frame rearraggements
80
60
40
20
0
Trβd1 Trβd2
E
DN3 Trβd–j rearrangements
% of in-frame rearraggements
25
20
15
10
5
0
Trβj1-1 Trβj1-2 Trβj1-3 Trβj1-4 Trβj1-5 Trβj1-6 Trβj1-7 Trβj2 Trβj2-1 Trβj2-2 Trβj2-3 Trβj2-4 Trβj2-5 Trβj2-6 Trβj2-7
F
Sorted DP: TCRα
TCRα rearrangements (c.f. β2m)
1
0.1
0.01
0.001
Jα58 Jα49 Jα31 Jα17 Jα2
TRAV12
TRAV13
TRAV14
TRAV17
TRAV19

217

218 **Figure 2.** Thymocytes of *PG* mice support diminished levels of *Tcrb* and *Tcra* recombination. **(A-B)**
219 Taqman qPCR quantification of rearrangements of each Vβ segment to DJβ1.1 (A) or DJβ2.1 (B)
220 complexes conducted on genomic DNA from DN3 thymocytes. Signals from each assay were normalized
221 to values from an assay for the invariant CD19 gene. Shown are average values +/- SEM from three
222 independent DN3 thymocyte preparations, each from a different mouse. **(C-E)** Adaptive Immunoseq
223 quantification of the percentage usage of each Vβ (C), Dβ (D), or Jβ (E) segment in *Tcrb* rearrangements
224 of DN3 thymocytes. Shown are average values from two independent DN cell preparations. **(F)** qPCR
225 quantification of specific Vα/Jα rearrangements peformed on genomic DNA from DP thymocytes.
226 Signals from each assay were normalized to values from an assay for the invariant β2m gene. Shown are
227 the average values +/- SEM from three independent DP cell preparations. For all graphs in figure: #, not
228 detected, n.s. $p>0.05$; * $p<0.05$, ** $p<0.01$, *** $p<0.001$, **** $p<0.0001$
229
230

231 **Reduced *Tcrb* gene assembly impairs DN thymocyte development in homozygous Rag1 P326G mice.**
232 The greater than normal number of DN3 thymocytes in *PG* mice is not typical of a mutation that impairs
233 V(D)J recombination and could reflect altered β-selection. Thus, to distinguish potential contributions of
234 reduced *Tcrb* gene assembly versus decreased pre-TCR-signaling, we conducted a more refined analysis
235 of DN stage cells based on CD28 protein expression. After successful *Tcrb* gene assembly in
236 $CD28^{-}CD25^{high}$ DN3a thymocytes, pre-TCR signaling drives differentiation of DN3b and then DN3c
237 thymocytes characterized by upregulation of CD28 and downregulation of CD25 (22). Mirroring relative
238 levels of *Tcrb* rearrangements in DN3 thymocytes, we observed decreased progression of DN3a cells to
239 the DN3b and DN3c stages, as well as a smaller fraction of DN3a cells expression TCRβ protein, in *PG*
240 mice relative to *WT* mice (Fig. 3, A - F). We compared the percentage of DN3a cells expressing TCRβ
241 protein to the percentage of these cells that develop into DN3b cells. We found equivalent values between
242 *PG* and *WT* mice (Fig. 3, G). We also compared the percentage of total DN3 cells expressing TCRβ protein
243 to the fraction of these cells that progress to the DN4 stage. Here again we found equivalent values between
244 *PG* and *WT* mice (Supplemental Figure 2). Together, these data provide no evidence for diminished pre-
245 TCR signaled development of β-selected DN3 thymocytes. Therefore, the most plausible explanation for
246 impaired DN thymocyte development in *PG* mice is decreased levels of TCRβ gene rearrangements.

Figure 3

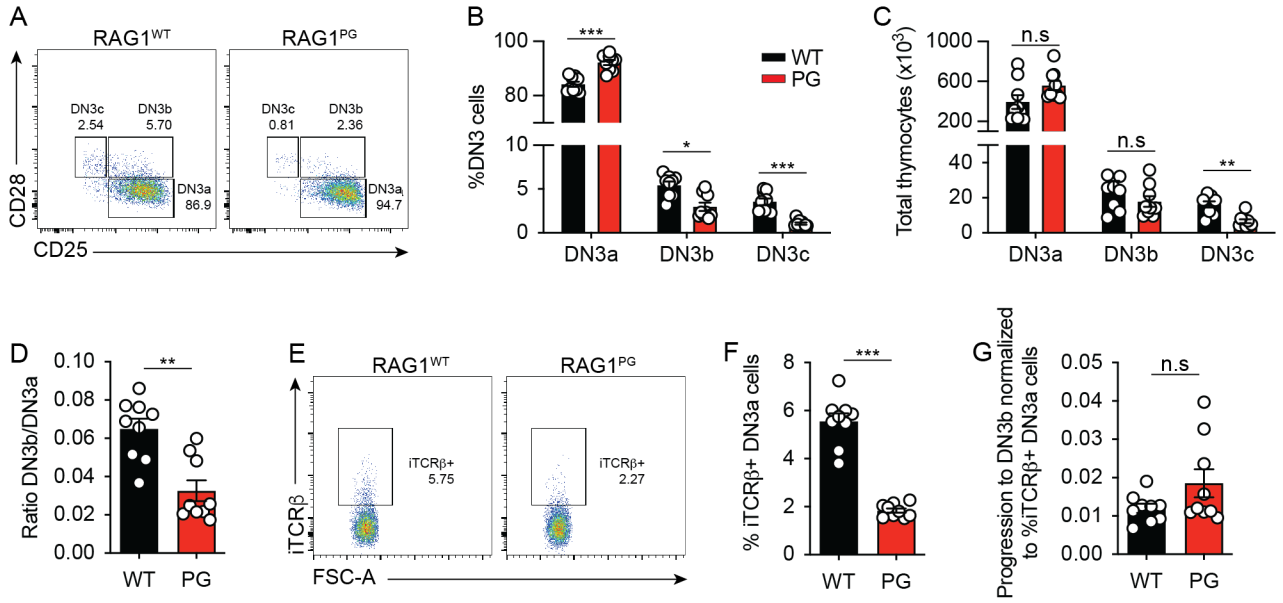

Figure 3. *PG* DN3 thymocytes exhibit normal efficiency of pre-TCR signaled differentiation. **(A)** Representative flow cytometry plots of DN3a, DN3b, and DN3c stages of thymocyte development showing the frequency of cells at each stage. **(B-C)** Quantification of percentages (E) or numbers (F) of total DN3 cells in each stage. Shown are all data points and average values +/- SEM from three independent experiments each with three mice of each genotype (n = 9 mice per genotype, analyzed by multiple t tests using the Holm-Sidak method; n.s. p>0.05, * p<0.05, ** p<0.005, **** p<0.00005). **(D)** Quantification of percentages of DN3a cells that progress into DN3b cells. Shown are all data points and average values +/- SEM from three independent experiments each with three mice of each genotype (n = 9 mice per genotype, analyzed by unpaired t-test with Welch's correction; **p<0.005). **(E)** Representative flow cytometry plots of intracellular TCRβ protein expression in DN3a thymocytes. **(F)** Quantification of percentages of DN3a cells expressing intracellular TCRβ protein. **(G)** Ratios comparing the percentages of DN3a cells expressing intracellular TCRβ protein to the percentages of DN3a cells that transition into DN3b cells. (**E-J**) Shown are all data points and average values +/- SEM from three independent experiments each with three mice of each genotype (n = 9 mice per genotype, analyzed by unpaired t-test with Welch's correction; n.s. p>0.05, *** p<0.0005).

263

264 **Homozygous Rag1 P326G mutation decreases the efficiencies of positive and negative selection of**

265 **conventional αβ T cells and differentiation of iNKT cells.**

266 In developing B cells, RAG DSBs generated during *Igk* gene assembly signal transcriptional regulation

267 of proteins that govern antigen receptor signaling, lymphocyte selection, cellular survival, and/or cellular

268 proliferation (23-25). Considering this and the decreased *Tcra* gene assembly in *PG* DP thymocytes, we

269 investigated whether any of the thymocyte selection and subsequent differentiation processes that depend

270 on αβ TCR signaling might be impaired in *PG* mice. As a proxy to evaluate positive selection in *PG* mice,

271 we determined the frequency of αβ TCR expressing (TCRβ^{+}) Stage 1 thymocytes that initiate positive

272 selection as indicated by progression to Stage 2 in *PG* and *WT* mice (Fig. 4 A). By analyzing only αβ

273 TCR expressing cells, we circumvent potential effects of decreased *Tcra* gene rearrangements reducing

274 the fraction of DP thymocytes that express αβ TCRs and are subject to selection. This frequency is lower

275 in *PG* mice (Fig. 4 B), consistent with modestly less efficient positive selection of αβ TCR expressing DP

276 thymocytes upon homozygous Rag1^{P326G} mutation. Yet, we note that this is an imperfect means to quantify

277 positive selection because it cannot account for possible differences in progression through subsequent

278 stages or cellular fate decisions from specific TCR/pMHC interactions. Thus, we also quantified numbers

279 of cells at each of the four stages of positive selection, finding fewer cells at each stage in *PG* mice relative

280 to *WT* mice (Fig. 4 C). Importantly, there is a greater decrease of cellularity in stage 2 (1.71x) as compared

281 to stage 1 (1.25x), indicating fewer cells are moving from stage 1 to stage 2 in *PG* mice. Finally, we

282 quantified CD69 expression and the ratio of CD69 to TCRβ expression at each stage as CD69 upregulation

283 correlates directly with αβ TCR signaling strength. Although we observed no difference of absolute levels

284 of CD69 expression, *PG* mice have decreased CD69 expression relative to TCRβ expression in stage 2

285 thymocytes that are initiating positively selection (Fig. 4 D). Collectively, these analyses indicate that αβ

286 TCR signaled upregulation of CD69 and positive selection is less efficient in *PG* mice. However, they do

287 not distinguish between potential effects from altered primary repertoires of *Tcrb* and *Tcra* genes versus
288 diminished intrinsic αβ TCR signaling capacity. They also do not address the possibility that the <10%
289 reduction in numbers of total thymocytes in *PG* mice alters thymic architecture in a manner that decreases
290 the fraction of DP cells that engage pMHC presented by TECs or DCs.
291

292

Figure 4

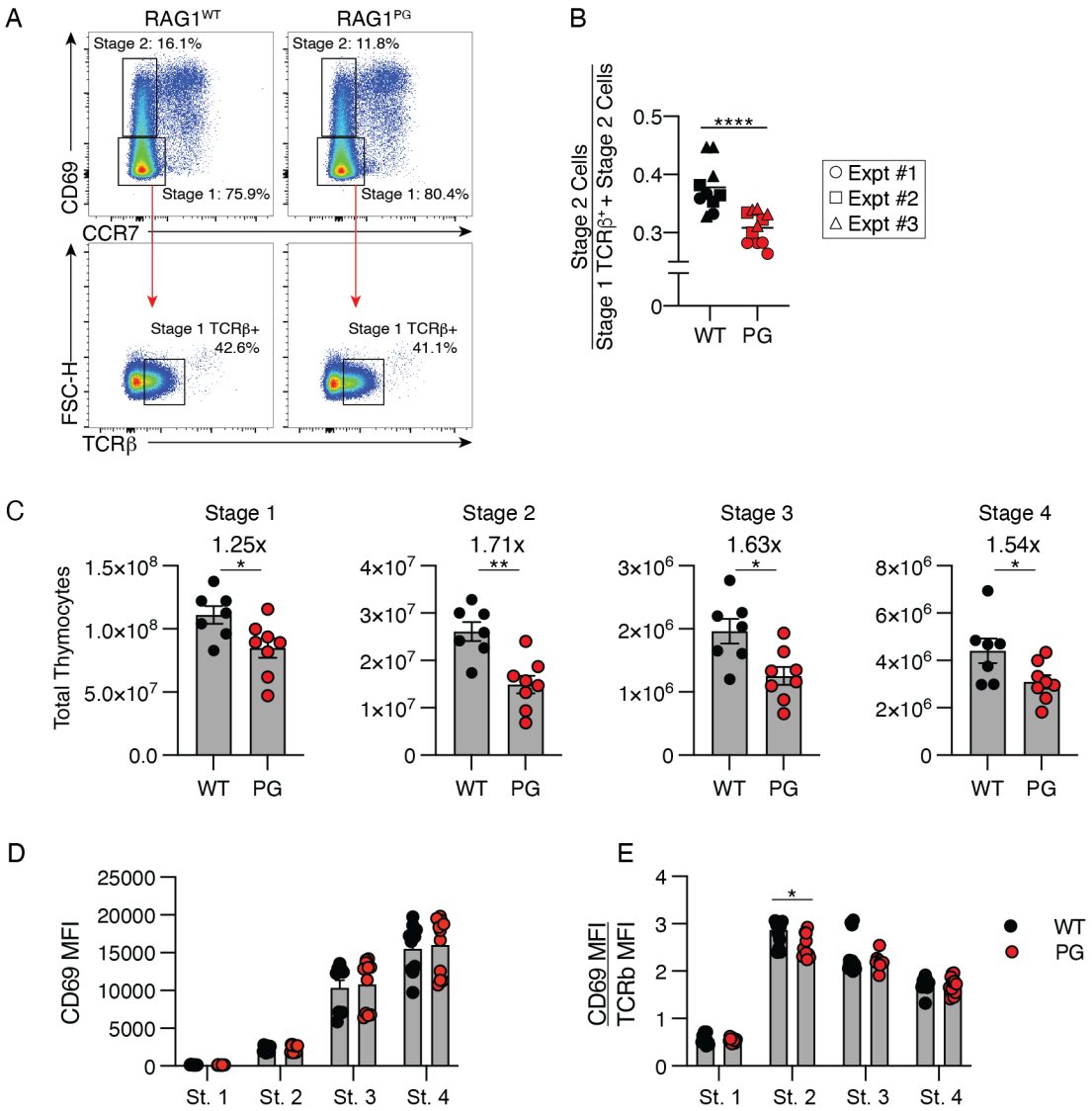

293

294 **Figure 4.** *PG* mice exhibit impaired positive selection. **(A)** Gating strategy for measuring positive
295 selection of thymocytes showing Stage 1 and 2 gates. The TCRβ$^+$ gate was set using wild-type thymocytes
296 by gating on live, singlet, CD4$^+$CD8$^+$ cells, preparing a histogram showing TCRβ staining on cells within
297 this gate, and gating on the shoulder that represents cells expressing TCRβ. **(B)** Quantification of the ratio
298 of the number of Stage 2 cells to the total number of Stage 1 and 2 cells. Shown are all data points and
299 global mean from three independent experiments (n = 10-11 mice per genotype, 2-way ANOVA indicating
300 effect of genotype). **(C)** Quantification of numbers of cells in each stage of positive selection. Dots

301 indicate individual mice. Data pooled from 2-independent experiments (n = 7-8 mice per genotype, bars
302 indicate mean +/- SEM analyzed by Man-Whitney test). (**D**) Quantification of CD69 expression alone and
303 in comparison to TCRβ expression on cells at each stage of positive selection. Dots indicate individual
304 mice. Data pooled from 2-independent experiments (n = 8 mice per genotype, bars indicate mean +/- SEM.
305 Analysed by 2-way ANOVA and Sidak multiple comparison post-test) For all graphs in figure: n.s.
306 $p>0.05$; * $p<0.05$, ** $p<0.01$, *** $p<0.001$, **** $p<0.0001$.
307
308

309 To determine whether the Rag1^{P326G} mutation impairs negative selection , we utilized a naturally occurring
310 system of superantigen-mediated negative selection (26). Laboratory mice express remnant mouse
311 mammary tumor virus (MMTV) retroviral products. Some of these products can bind the MHCII I-E^{d}
312 protein and certain Vβ peptides, including Vβ5.1-5.2 (encoded by *Trbv12.1-12.2*) and Vβ12 (encoded by
313 *Trbv15*), to trigger exceptionally strong αβ TCR signaling that promotes negative selection (26, 27). Our
314 sequencing analysis of *Tcrb* gene rearrangements in DN3 thymocytes shows equivalent representation of
315 *Trbv12.1*, *Trbv12.2*, and *Trbv15* in the primary Vβ repertoire (Fig. 2 C). Considering that Vβ repertoire
316 remains constant during DN-to-DP thymocyte development (28), assaying superantigen-mediated
317 deletion of Vβ5.1-5.2 or Vβ12 accounts for differences of Jβ repertoire of *Tcrb* genes assembled in *WT*
318 and *PG* mice. Moreover, the reduced level and altered repertoire of *Tcra* genes assembled in DP cells of
319 *PG* mice would not influence superantigen-mediated deletion of thymocytes expressing αβ TCRs with
320 specific Vβ peptides. BALB/c, but not C57BL/6, strain mice express I-E^{d} protein. As a result, thymocytes
321 expressing Vβ5.1-5.2 or Vβ12 are efficiently deleted in BALB/c, but not B6, genetic backgrounds. We
322 bred BALB/c background *Rag1*$^{-/-}$ mice with C57BL/6 background Rag1 *PG* or *WT* mice to generate and
323 analyze *Rag1*$^{PG/-}$ and *Rag1*$^{WT/-}$ mice expressing I-E^{d} protein. To ascertain whether these mice exhibit a
324 difference in superantigen-mediated negative selection, we measured the frequencies of DP thymocytes
325 that have not completed αβ TCR selection and post-selection SP thymocytes expressing I-E^{d}:MMTV-
326 reactive (Vβ5^{+} or Vβ12^{+}) or -unreactive (Vβ6^{+}, Vβ8^{+}, or Vβ14^{+} encoded by *Trbv19*, *Trbv13.1-13.3*, or
327 *Trbv31*, respectively) αβ TCRs (Fig. 5, A-F). We calculated the percentages of DP and SP thymocytes
328 expressing each Vβ peptide (Fig. 5, B-F). Our analysis indicates that greater fractions of I-E^{d}:MMTV-
329 reactive thymocytes proceed through DP-to-SP development in *Rag1*$^{PG/-}$ mice as compared to *Rag1*$^{WT/-}$
330 mice (Fig. 5, B, C, and G), consistent with impaired negative selection of highly self-reactive thymocytes.
331 In contrast, we found that the types of un-reactive thymocytes assayed develop equivalently in each
332 genotype (Fig. 5, D -G). While the latter finding does not reflect less efficient positive selection, we note

333 that this experiment monitors a small subset of thymocytes expressing specific Vβ peptides and thus is
334 not as sensitive as determining the frequencies of overall DP thymocytes that initiate positive selection.
335 Regardless, the data indicate that *PG* mice exhibit less efficient deletion of thymocytes that express
336 αβ TCRs containing superantigen-reactive Vβ peptides. As Vβ repertoire is normal in *PG* mice (Fig. 2C),
337 plausible explanations for this impaired form of negative selection include that intrinsic αβ TCR signaling
338 capacity is dampened and/or reduced numbers of DP thymocytes prevents some from contacting or
339 maintaining interaction with superantigen.
340

Figure 5

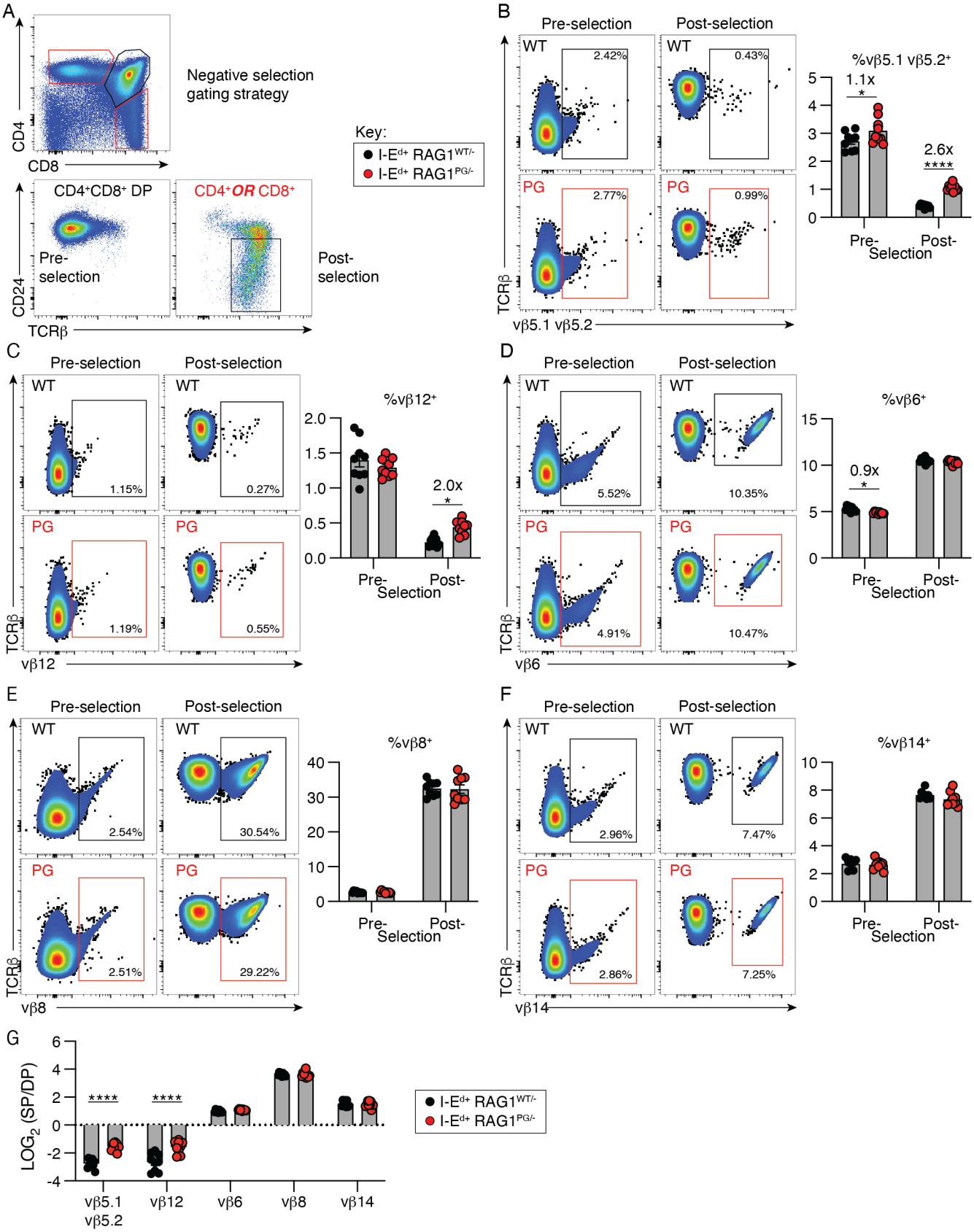
A
CD4
CD8
Negative selection gating strategy
CD4+CD8+ DP
Pre-selection
CD4+ OR CD8+
Post-selection
CD24
TCRβ
Key:
I-Ed+ RAG1WT/-
I-Ed+ RAG1PG/-
B
Pre-selection
Post-selection
WT
PG
2.42%
0.43%
2.77%
0.99%
%vβ5.1 vβ5.2+
1.1x
2.6x
Pre-Selection
Post-Selection
vβ5.1 vβ5.2
C
1.15%
0.27%
1.19%
0.55%
%vβ12+
2.0x
vβ12
D
5.52%
10.35%
4.91%
10.47%
%vβ6+
0.9x
vβ6
E
2.54%
30.54%
2.51%
29.22%
%vβ8+
vβ8
F
2.96%
7.47%
2.86%
7.25%
%vβ14+
vβ14
G
LOG2 (SP/DP)
vβ5.1 vβ5.2
vβ12
vβ6
vβ8
vβ14

341

342 **Figure 5.** *PG* mice exhibit impaired superantigen-mediated negative selection. **(A)** Gating strategy form
343 measuring negative selection of specific $V\beta^+$ thymocytes in F1 progeny of C57BL/6 background *WT* or
344 *PG* mice crossed with BALB/c background $Rag1^{-/-}$ mice. Pre-gated on live singlets. **(B-F)** Representative
345 analyses and quantification of the indicated $V\beta^+$ cells in DP thymocytes that have not completed αβ TCR
346 selection or post-selection SP thymocytes. **(G)** Data from B-F displayed as LOG_2 ratio of respective
347 percent $V\beta^+$ cells in SP versus DP gates. Shown are all data points and average +/- SEM from two
348 independent experiments (n = 9 mice per genotype 2-way ANOVA with Sidak multiple comparison post-
349 test). For any significantly different combinations, fold change is indicated. For all graphs in figure: *
350 $p<0.05$, **** $p<0.0001$.
351
352

353 Finally, to ascertain potential effects of Rag1^{P326G} mutation on agonist selection, we focused on assaying
354 iNKT cell development because their limited TCR diversity and specificity facilitates their identification
355 and assays of their selection and differentiation subsequent to V(D)J recombination. This lineage develops
356 when TCRs containing an invariant Vα14-Jα18 TCRα chain and TCRβ chains with Vβ regions encoded
357 by *Trbv1*, *Trbv13.1-13.3*, or *Trbv19* bind lipids presented by the MHC-like CD1d protein on different DP
358 thymocytes (29-31). These interactions induce strong TCR signals that mediate agonist selection of DP
359 cells into αβ TCR-expressing iNKT common progenitor (Stage 0) cells and their differentiation into iNKT
360 precursor (Stage 1) cells and then into different mature effector subsets (iNKT1, iNKT2, or iNKT17)(32).
361 We first used a CD1d tetramer loaded with PBS57, an analogue of the α-galactosylceramide (α-GalCer)
362 glycolipid, to identify α-GalCer-reactive iNKT lineage cells in *WT* and *PG* mice. Unloaded "empty"
363 tetramer showed little to no staining in any of the samples (exemplified in Fig. 6A). As compared to *WT*
364 mice, *PG* mice had fewer absolute numbers of thymic α-GalCer-reactive iNKT lineage cells (Fig. 6, A
365 and B). While *PG* mice also tended to have fewer splenic iNKT cells (Fig. 6, A and B), this difference
366 did not reach statistical significance (p=0.06) with the numbers of mice analyzed. We used Taqman PCR
367 to show that the levels of Vα14-to-Jα18 rearrangements in sorted DP thymocytes of *PG* mice are ~10%
368 relative to *WT* mice (Fig. 6 C), which is consistent with reduced generation of Vα14-Jα18 TCRα chains
369 contributing to the lower numbers of thymic α-GalCer-reactive iNKT cells in *PG* mice. However, we
370 observed no significant differences in the numbers of PBS57 loaded tetramer-staining cells at both Stage
371 0 (CD24^{hi}CD44^{-}NK1.1^{-}) or Stage 1 (CD24^{lo}CD44^{-}NK1.1^{-}) in *WT* and *PG* mice (Fig. 6, D and E),
372 indicating that the reduction of Vα14-to-Jα18 rearrangements in *PG* DP thymocytes does not translate
373 into decreased agonist selection of α-GalCer-reactive iNKT lineage cells. In contrast, we observed that
374 *PG* mice have lower numbers of NKT2/17 (CD24^{lo}CD44^{+}NK1.1^{-}) and NKT1 (CD24^{lo}CD44^{+}NK1.1^{+})
375 effector iNKT cells that develop from Stage 1 precursor cells (Fig. 6, D and E). Notably, the median
376 fluorescence intensities of TCRβ expression and PBS57/CD1d tetramer binding of thymocytes was

377 similar or slightly higher in *PG* mice relative to *WT* mice (Fig. 6 A, data not shown), indicating that α-
378 GalCer-reactive iNKT cells of *PG* mice have a normal range of intrinsic affinity for this lipid presented
379 by CD1d. We also analyzed iNKT populations in the competitive setting of mixed bone marrow chimeras
380 comparing mice that received donor bone marrow that was either 100% *PG* or at 1:1 mix of *PG* and *WT*
381 marrow. The *WT* cells in the mixed chimeras outcompeted the *PG* cells starting at Stage 1 with more
382 pronounced effects in the terminally differentiated effector iNKT cell types (Supplemental Figure 1). The
383 same effect can be seen from the few remnant *WT* cells in the 100% *PG* recipient mice (Supplemental
384 Figure 1, C). These data indicate that there is a cell-intrinsic loss of fitness in iNKT cell development in
385 *PG* cells as they progress from Stage 0 to Stage 1 that is not revealed in the non-competitive environment.
386 Because the fitness of the *PG* iNKT Stage 0 and 1 cells is poor in the 1:1 mixed environment, it is difficult
387 to assess cell-intrinsic iNKT differentiation in this setting. Yet, the few remnant *WT* cells in the 100% *PG*
388 recipient mice continue to incrementally outcompete *PG* cells in both NKT1 and NKT 2/17 differentiation,
389 demonstrating a cell-intrinsic differentiation defect in this system. The basis for this defect could include
390 altered αβ TCR signaling arising from differences in Dβ-, Jβ-, CDR3β-, or CDR3α-encoded amino acids,
391 diminished RAG DSB-signalled changes in expression of proteins that control iNTK cell differentiation,
392 or both.

Figure 6

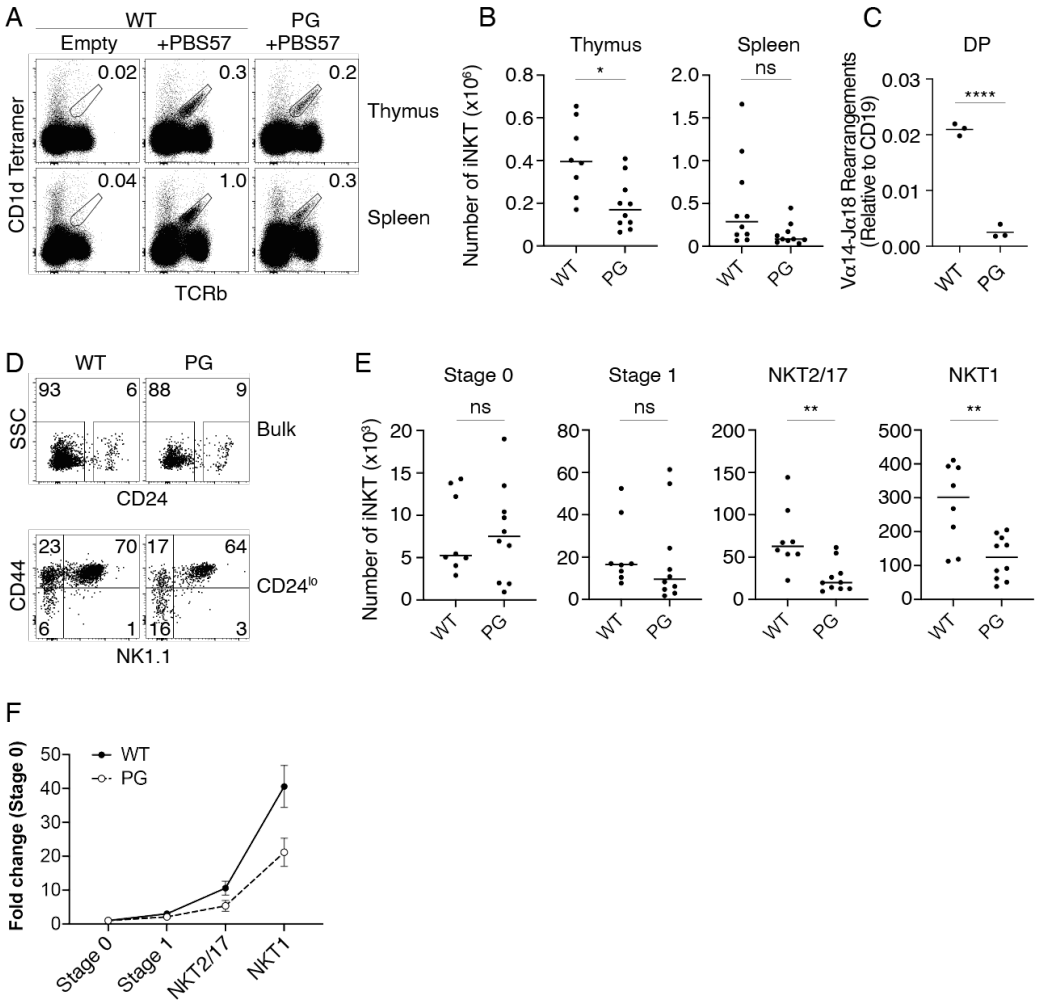

Figure 6. *PG* mice have impaired agonist selection of iNKT cells. (**A-B)** Representative flow cytometry plots (**A**) and quantification (**B**) of PBS57/CD1d tetramer binding iNKT cells in thymuses or spleeens. Gated on live, singlet lymphocytes. "Empty" denotes unloaded tetramer staining. (**B**) Data from three independent experiments with 1-4 mice per group. Mann-Whitney test: *, p=0.01 (thymus); ns, not significant (spleen). (**C**) Taqman PCR quantification of Vα14-Jα18 rearrangements from sorted DP thymocytes. The data were generated from three technical replicates of three independent biological samples from mice of each genotype. Data are represented as Mean +/- SEM analyzed by an unpaired parametric t test with Welchs correction. p<0.001. (**D-E)** Representative flow cytometry plots and gating strategy (**D**) or quantification (**E**) of Stage 0 ($CD24^{hi}$ CD44-NK1.1-), Stage 1 (CD44-NK1.1-), NKT2/17 (CD44+NK1.1-), and NKT1 (CD44+NK1.1+) iNKT cells.

404

405 **Mature αβ T cells of homozygous Rag1 P326G mice exhibit normal responses to activation.**

406 RAG endonuclease activity during lymphocyte ontogeny triggers permanent changes in gene expression
407 that correlate with impaired responses of mature lymphocytes (33). Considering that RAG endonuclease
408 function is diminished in thymocytes of *PG* mice, we sought to elucidate whether the mature αβ T cells
409 of these animals have normal or altered response to activation. We first conducted *in vitro* analyses. Upon
410 stimulation with PMA and ionomycin, splenic $CD44^{hi}$ αβ T cells from *PG* mice produce normal levels of
411 IFNγ, TNFα, IL-2, and IL-17A (Fig. 7 A). These cells also show normal proliferation upon anti-CD3/anti-
412 CD28 stimulation (Fig. 7 B). Moreover, stimulated $CD4^+$ and $CD8^+$ αβ T cells of *PG* mice normally
413 express their canonical transcription factors (Fig. 7, C and D) and cytokines (Fig. 7, E and F) when cultured
414 in respective skewing conditions. We next monitored αβ T cell responses *in vivo* following infection of
415 mice with an acute strain of lymphocytic choriomeningitis virus (LCMV-Armstrong). We analyzed mice
416 either seven days later to monitor at the immune response peak or 35 days later to monitor memory cells.
417 At each timepoint, we detected similar frequencies and numbers of antigen-specific $CD8^+$ αβ T cells that
418 stain with gp33:H-2Db tetramer in *PG* and *WT* mice (Fig. 7 G), indicating that *PG* mice display normal
419 numbers and dynamic responses of αβ T cells that recognize LCMV-Armstrong. We also observed
420 equivalent dynamic expression of Tbet, Eomes, KLRG1, and CD127 proteins on αβ T cells from *PG* and
421 *WT* mice (Fig. 7 H), indicating normal contraction of short-lived effector cells (SLECs), and sustained
422 memory/memory precursor effector cells (MPECs) in *PG* mice. Finally, we detected similar numbers of
423 antigen specific αβ T cells able to respond to the gp33, NP396, or gp61 viral peptides within a peptide re-
424 stimulation assay (Fig. 7, I and J). Together, these data demonstrate that the mature αβ T cells of *PG* mice
425 have normal responses to activation, in the tested conditions.

Figure 7

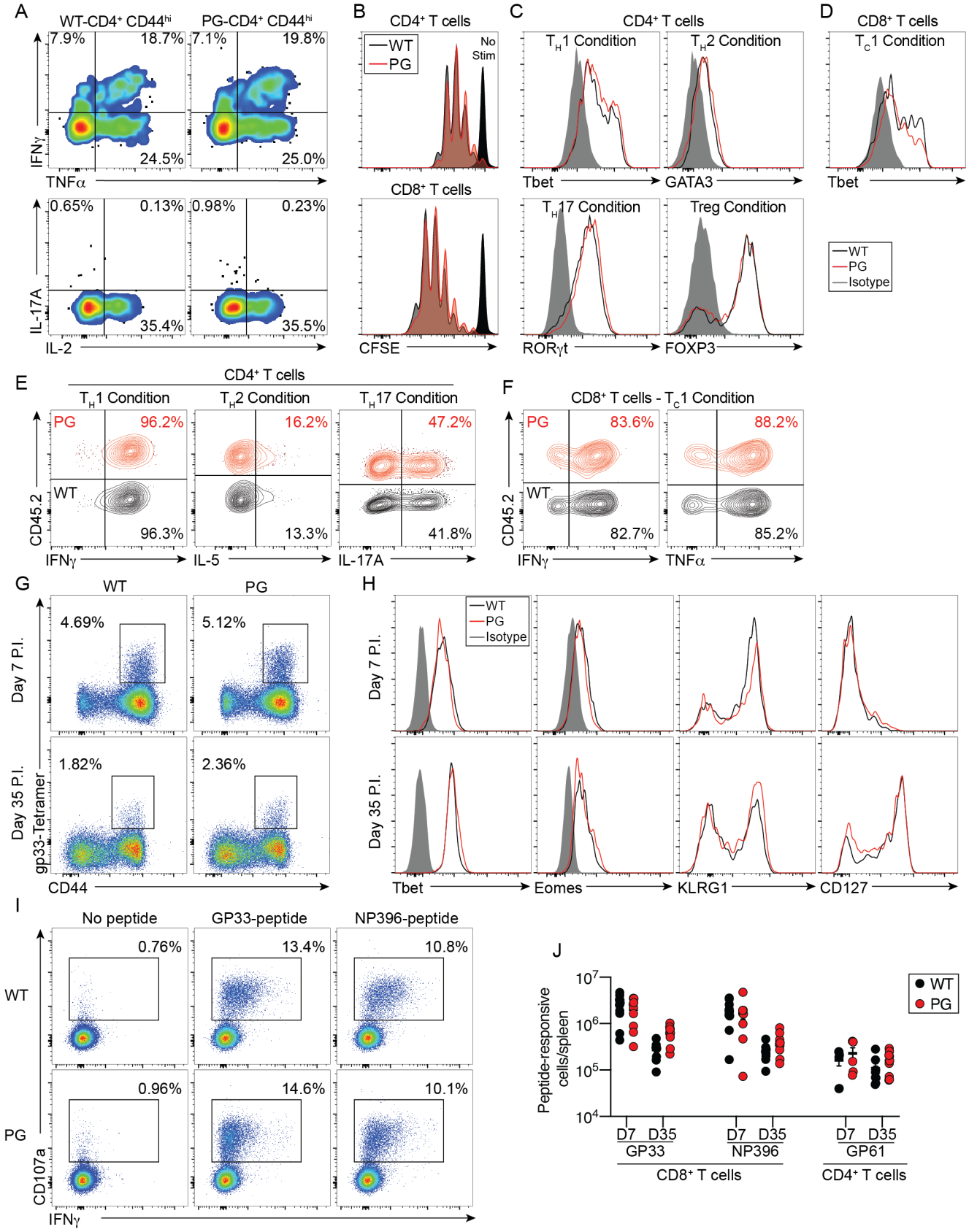
A
WT-CD4+ CD44hi
PG-CD4+ CD44hi
7.9%
18.7%
24.5%
7.1%
19.8%
25.0%
IFNγ
TNFα
0.65%
0.13%
35.4%
0.98%
0.23%
35.5%
IL-17A
IL-2
B
CD4+ T cells
WT
PG
No Stim
CD8+ T cells
CFSE
C
CD4+ T cells
TH1 Condition
TH2 Condition
Tbet
GATA3
TH17 Condition
Treg Condition
RORγt
FOXP3
D
CD8+ T cells
TC1 Condition
Tbet
WT
PG
Isotype
E
CD4+ T cells
TH1 Condition
TH2 Condition
TH17 Condition
PG
96.2%
16.2%
47.2%
WT
96.3%
13.3%
41.8%
CD45.2
IFNγ
IL-5
IL-17A
F
CD8+ T cells - TC1 Condition
PG
83.6%
88.2%
WT
82.7%
85.2%
CD45.2
IFNγ
TNFα
G
WT
PG
Day 7 P.I.
4.69%
5.12%
Day 35 P.I.
1.82%
2.36%
gp33-Tetramer
CD44
H
WT
PG
Isotype
Day 7 P.I.
Day 35 P.I.
Tbet
Eomes
KLRG1
CD127
I
No peptide
GP33-peptide
NP396-peptide
WT
0.76%
13.4%
10.8%
PG
0.96%
14.6%
10.1%
CD107a
IFNγ
J
Peptide-responsive cells/spleen
10^7
10^6
10^5
10^4
WT
PG
D7 D35
GP33
D7 D35
NP396
D7 D35
GP61
CD8+ T cells
CD4+ T cells

426

427 **Figure 7.** Mature αβ T cells of PG mice exhibit normal immune response. **(A)** Representative plot of
428 cytokine expression on $CD4^{+}CD44^{hi}$ αβ T cells following *ex vivo* stimulation of splenocytes with PMA
429 and ionomycin. **(B-F)** Representative analyses of naïve splenic $CD4^{+}$ or $CD8^{+}$ T cells after *ex vivo*
430 simulation with anti-CD3/anti-CD28 antibodies and additional antibodies to skew towards indicated
431 lineages. Shown is CFSE incorporation (B) or expression of relevant transcription factors (C, D) or
432 cytokines (E, F). **(G, H)** Representative flow data showing (G) frequencies of splenic αβ T cells that stain
433 with the gp33:H-2Db tetramer or (H) express indicated cytokines after LCMV infection of mice. Data are
434 representative of two independent experiments with at least four mice of each genotype. **(I, J)**
435 Representative plots (J) and (I) quantification of antigen-specific αβ T cells able to respond to indicated
436 viral peptides within a peptide re-stimulation assay. (A-F) Data are representative of two independent
437 experiments. (G-J) Data are combined from four independent experiments (two D7 and two D35
438 timepoints) with 8-11 mice of each genotype per time-point.
439
440

441 **Mature αβ T cells of homozygous Rag1^{P326G} mice exhibit increased autoimmune potential.**

442 Within a setting of less efficient negative selection as with homozygous Rag1^{P326G} mutation, an increased
443 predisposition to αβ T cell mediated autoimmunity would be expected. However, we did not observe overt
444 autoimmune symptoms within *PG* mice, possibly because mice of the C57BL/6 background are resistant
445 to spontaneous autoimmune diseases (34, 35). Thus, to investigate whether the Rag1^{P326G} mutation can
446 predispose to autoimmunity, we utilized an induced model of autoimmune colitis in C57BL/6 mice.

447

448 The colitis model involves transferring into *Rag1*$^{-/-}$ mice naïve CD4^{+} effector αβ T cells, which become
449 activated and trigger cytokine-driven colitis and associated systemic pathologies including weight loss
450 due to the absence of Tregs (36-38). We observed accelerated wasting of *Rag1*$^{-/-}$ mice receiving *PG* cells
451 relative to *WT* cells or no transfer (Fig. 8 A). We analyzed mice at eight weeks after transfer. As compared
452 to *WT* recipients, we detected greater numbers of total splenic CD4^{+} T cells and of CD4^{+} T cells producing
453 IFNγ, TNFα, and/or GM-CSF cytokines (Fig. 8, B and C). Colon length is used as a measure of disease
454 severity in this model, and mice receiving transferred *PG* cells had shorter colons relative to mice
455 receiving *WT* cells, consistent with worse disease caused by *PG* cells (Fig. 8 D). Histologic assessment
456 and scoring in this colitis model has been formalized (38), and can be grossly broken down into scores
457 related to inflammatory cell infiltration and scores related to injury of tissue architecture. There was no
458 statistical difference in inflammation scores between mice receiving *WT* and *PG* cells. However, tissue
459 damage scores were higher in mice receiving *PG* cells, suggesting that, on a per cell basis, *PG* cells induce
460 greater tissue injury in this model (Fig. 8, E-F). Notably, specifically in *PG*-transferred animals, we
461 observed autoimmune pathologies in addition to colitis, including dermatitis, chylous ascites, severe small
462 intestine enlargement, and neurological distress (Fig. 8 H). Dermatitis was most common and involved
463 massive inflammatory infiltration and tissue damage (Fig. 8 I). Consistent with more widespread
464 autoimmune conditions in *PG*-transferred mice, we observed significant splenomegaly in these mice (Fig.
465 8 J). Finally, while not statistically significant, we observed an increased rate of premature death in the

466 mice transferred with *PG* cells compared to *WT* cells (Fig. 8 K), which was especially surprising because

467 death is an unexpected outcome in this model. Collectively, the data from this colitis model indicate that

468 $CD4^+$ effector T cells from *PG* mice have greater than normal intrinsic autoimmune potential.

469

Figure 8

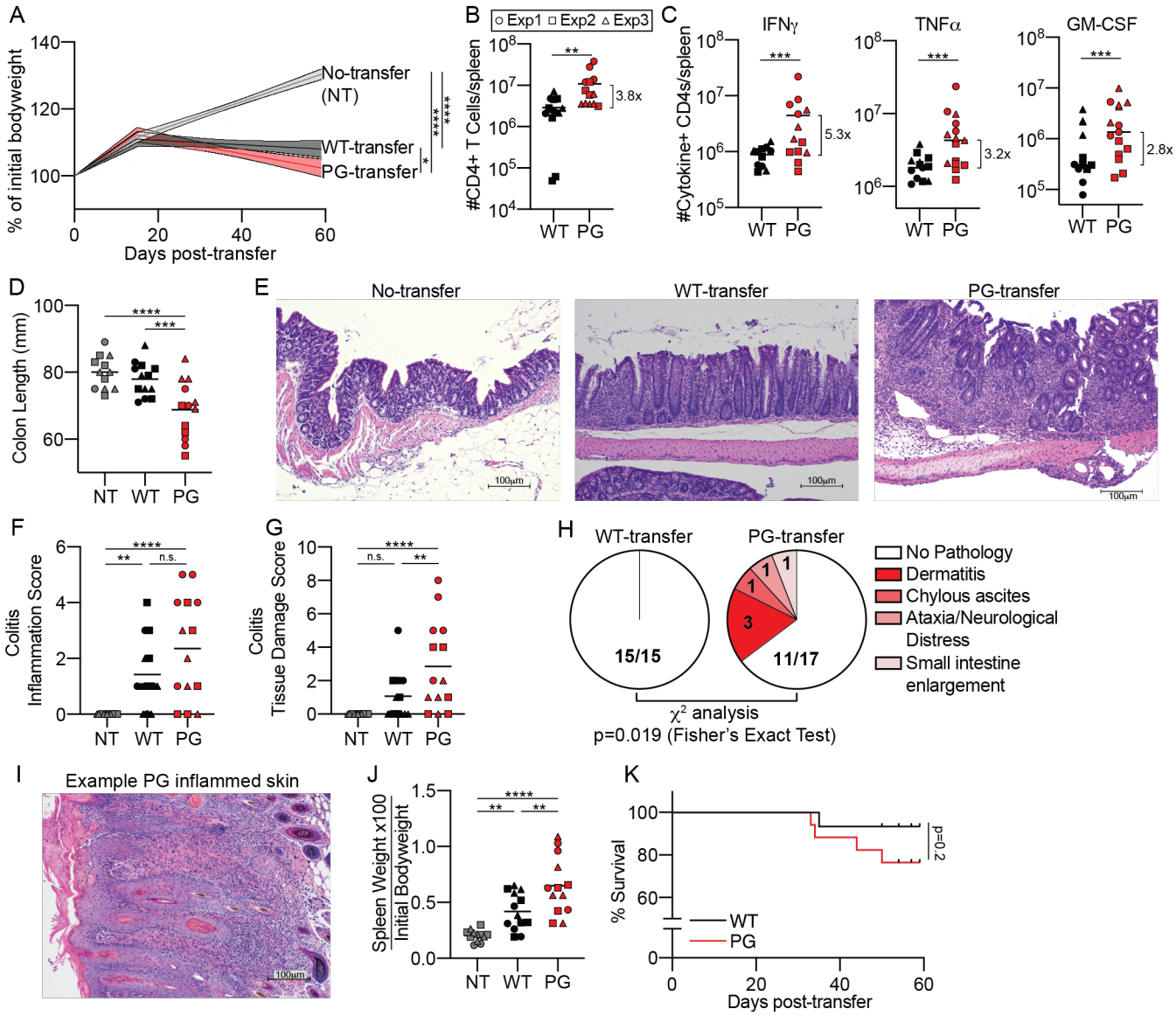

470

471 **Figure 8.** Mature αβ T cells of *PG* mice possess higher than normal autoimmune hazard**. (A)** Graph of

472 body weights of *Rag1*$^{-/-}$ hosts over time after transfer of *WT* or *PG* $CD4^+$ T cells or no cells (NT). Data

473 combined from three independent experiments with a total of 13-17 mice of each genotype. Lines indicate

474 fitted segmented-linear regression lines +/- 95% confidence interval. Day 15 was fixed as the inflection

475 point. Difference between gradients of second slope was determined by linear regression analysis. **(B)**
476 Numbers of $CD4^+$ T cells in spleen eight weeks post-transfer. **(C)** Total number of IFNγ, TNFα, and/or
477 GM-CSF producing cells per spleen. Shown are all data points from three independent experiments with
478 12-14 mice per group. Bar indicates global mean. Pre-gating on live singlets, $CD90.2^+$, $CD4^+$, and $CD44^+$.
479 **(D)** Colon length of mice sacrificed at eight weeks post-infection. **(E)** Representative hemotoxylin and
480 eosin stained colon sections from respective mice at eitght weeks post-transfer. 10x magnification. **(F-G)**
481 Total colitis score as assessed by blinded pathologist. Scored as per previously described guidelines for
482 the five phenotypes (38): (F) Colon inflammation score (contribution of scores for crypt abcesses and
483 inflammatory cell infiltrate). (G) Colon tissue damage score (contribition of scores for crypt architecture,
484 tissue damage, goblet cell loss). **(H)** Non-colitis pathologies described for mice transferred with *WT* versus
485 *PG* cells. **(I)** Hemotoxylin and eosin stained skin section from *PG*-transferred mouse with severe
486 dermatitis at eight weeks post-transfer. 10x magnification. **(J)** Spleen weight at eight weeks post-transfer
487 normalized to total mouse bodyweight prior to transfer. **(K)** Survival curves of mice transferred with *WT*
488 or *PG* cells. Data combined from three independent experiments. Statistical analysis = Log-rank Mantel-
489 Cox test. Overall: 0/13 NT mice died, 1/15 *WT*-transferred mice died, and 4/17 *PG*-transferred mice died.
490 (B, C, F, G, and J) Shown are all data points from three independent experiments, 12-14 mice per group.
491 Experiment indicated by shape of data point. Bar indicates global mean. Analyzed by 2-way ANOVA
492 with Tukey HSD post-test. n.s. $p>0.05$; * $p<0.05$, ** $p<0.01$, *** $p<0.001$, **** $p<0.0001$
493

494 **Discussion**

495

496 Our analysis of *PG* mice demonstrates that the RAG1 RING domain stimulates V(D)J recombination of
497 endogenous TCR loci and resulting αβ T cell development *in vivo*. The decreased V(D)J recombination
498 activity in PG mice manifests as lower levels of Vβ-to-DJβ and Vα-to-Jα rearrangemetns within DN and
499 DP thymocytes, respectively. These reduced Vβ rearrangements diminish overall progression of the DN3
500 thymocyte population to the DN4 and then DP stage by lowering the frequency of DN3 cells that create
501 TCRβ protein. Similarly, reduced Vα rearrangements likely contribute to less efficient overall positive
502 selection of the DP thymocye population by lowering the frequency of DP cells that establish αβ TCRs.
503 Moreover, the 10% lower numbers of DP thymocytes in *PG* mice resulting from decreased expansion of
504 the DN population could impair positive selection by reducing engagement of αβ TCRs on DP cells with
505 pMHC on TECs or DCs. Our data align with the recent report that $Rag1^{P326G}$ mutation in mice diminishes
506 V(D)J recombination of IgH and Igκ loci and the B cell developmental transitions that depend on these
507 rearrangements by reducing RAG cleavage (19). The $Rag1^{P326G}$ mutation might intrinsically decrease
508 RAG endonuclease activity by altering Rag1 protein structure and/or impairing Rag1-mediated
509 autoubiquitylation of RAG complexes (10, 11, 15). As the RAG1 RING domain promotes ubiquitylation
510 of histone H3 proteins (12-14), our data raise the possibility that the RAG1 ubiquitin ligase might stimulate
511 accessibility of chromatin over TCR and Ig loci to enhance RAG binding, cleavage, or both. Moreover,
512 because RAG1 RING domain mutations that impair histone H3 ubiquitylation result in accumulation of
513 coding ends and signal ends in episomal substrates (13), less efficient V(D)J coding join formation might
514 diminish TCR and Ig gene rearrangements and resulting lymphocyte differentation in *PG* mice.
515 Eludicating the precise molecular mechanisms by which the RAG1 RING domain promotes V(D)J
516 recombination *in vivo* requires biochemical studies of RAG complexes in *WT* and *PG* cells, epigenetic

517 analyses of TCR and Ig loci in mice that express endonuclease-inactivated RAG complexes with or
518 without Rag1^{P326G} mutation, and characterization of the ubiquitylated proteome in all four cell types.
519
520 Our analysis of *PG* mice also reveals that the RAG1 RING domain shapes primary TCR gene repertoires
521 and might thereby regulate positive selection and negative selection of conventional αβ T cells. The amino
522 acids encoded by rearranged gene segments or *de novo* CDR3 nucleotoides influence antigen recognition,
523 signaling, and selection of αβ TCRs. Although we did not analyze CDR3 nucleotoides, our data indicate
524 differences in utilization of Dβ and Jβ segments within Vβ-to-DJβ rearrangements and Vα and Jα
525 segments within Vα-to-Jα rearrangements between *WT* and *PG* mice. The altered utilization of TCRβ
526 and/or TCRα gene segments in V(D)J rearrangements of *PG* mice might create a primary TCR repertoire
527 that overall is less efficient at promoting positive selection. Moreover, the altered usage of TCRβ and/or
528 TCRα gene segments in *PG* mice could produce a TCR repertoire with a greater than normal frequency
529 of highly selfreactive receptors that escapes negative selection. Decreased RAG endonuclease activity
530 from Rag1^{P326G} mutation likely reduces the utilization of Dβ2 and 3'Jαs by lowering the frequency of V
531 recombination to these gene segments after V recombination to Dβ1 or 5'Jαs. One prediction of impaired
532 RAG cleavage activity is elevated usage of gene segments with stronger RAG-targeting recombination
533 signal sequence (RSS) elements (20). This is the case for Vβ usage in mice with profoundly low RAG
534 endonuclease activity caused by a deletion of the RING domain and all more N-terminal residues (21).
535 The Jβ2.5 gene segment has a stronger RSS than Jβ2.2 (39). Considering that Jβ2.5 usage increases and
536 Jβ2.2 usage remains normal in TCRβ gene rearrangements of *PG* mice, Rag1^{P326G} mutation likely alters
537 Jβ utilization by means other than reducing RAG endonuclease activity. The mutation could prevent the
538 RAG1 ubiquitin ligase from promoting accessibility of some Jβ RSSs, destablilize snynaptic complexes
539 based on distinct properties of participating Jβ RSSs, or both. The same approach needed to elucidate how

540 the RAG1 RING domain promotes V(D)J recominaiton *in vivo* would provide mechanistic insights into
541 how it also shapes primary antigen receptor gene repertoires.
542
543 Although further experimentation is required to better understand how the RAG1 RING domain regulates
544 V(D)J recombination, any discussion of αβ TCR selection and resultant differentiation of DP thymocytes
545 would be incomplete without consideration of a possibilities that the RAG1 RING domain regulates these
546 processes independent of assembling TCR genes. The impaired superantigen-mediated negative selection
547 of conventional αβ T cells and differentiation of iNKT lineage cells in *PG* mice suggest potential functions
548 of the RAG1 RING domain beyond stimulating and shaping TCR gene rearrangements. The molecular
549 basis for superantigen-mediated negative selection is that these antigens interact simultaneously with
550 MHC proteins on TECs and particular Vβ peptides on DP thymocytes to illicit very strong TCR signaling
551 that triggers apoptosis. To our knowledge, there is no evidence that Dβ-, Jβ-, CDR3β-, Vα, Jα, or CDR3α-
552 encoded amino acids influence superantigen-directed negative selection. Thus, as Vβ usage within Vβ-to-
553 DJβ rearrangements is normal in *PG* mice, the altered Dβ, Jβ, Vα, and Jα usage should not impair
554 superantigen-driven negative selection of DP thymocytes that express relevant Vβ peptides within their
555 αβ TCRs. How iNKT cell subsets develop from agonist-selected iNKT progenitor cells remains
556 incompletely understood. A recent study in mice expressing αβ TCRs from a single pre-assembled Vα14-
557 Jα18 rearrangement formulated a model that iNKT cell development is a two step process where the first
558 step involves transient uniform TCR signaling that drives agonist selection of DP thymocytes into iNKT
559 common precursors and the second step involves antigen/TCR-independent differentiation of different
560 mature effector subset through differential gene expression (40). However, this study did not investigate
561 the effects of TCR signaling strength on differentiation of iNKT precursor cells. Prior work that the
562 development of NKT2 and NKT17 but not NKT1 cells is impaired by a hypomorphic mutation of the
563 Zap70 TCR signaling protein that weakens TCR signaling supports the notion that strength of TCR

564 signaling influences iNKT cell differentiation (40). Although TCRβ amino acids encoded by Jβ segments
565 and CDR3β nucleotides influence αβ TCR specifity of iNKT cells (41), it is hard to explain how the minor
566 changes in Dβ and Jβ usage in *PG* mice would substantially alter TCR signaling to impair the generation
567 of iNKT subtypes from iNKT precursor cells.
568
569 We envision two not-mutually exlusive possibilities that account for the impaired superantigen-mediated
570 negative selection of conventional αβ T cells and differentiation of NKT precursor cells in *PG* mice. One
571 is that the 10% reduction in DP thymocyte numbers decreases frequencies or durations of αβ TCR contacts
572 with pMHC on other thymic cells or CD1d/lipid complexes on other DP cells, causing weaker or otherwise
573 different TCR signaling. The second possibility is that Rag1^{P326G} mutation modifies the expression and/or
574 activities of proteins in DP thymocytes and derivative iNKT precursor cells. To explore this latter scenario,
575 we quantified Zap70 expression because reduced Zap70 protein levels and/or activity impairs positive and
576 negative selection (42-44), as well as iNKT cell differentiation (45, 46). We detected lower levels of Zap70
577 protein but not mRNA in DP cells of *PG* mice at each of the four stages of αβ TCR-signaled positive
578 selection as defined by CD69 and CCR7 protein expression (Supplemental Figure 3). Zap70 proteins
579 levels are normal in splenic αβ T cells of *PG* mice, correlating with a time point when *Rag1* is not
580 expressed and therefore should not be able to directly influence protein levels (Supplemental Figure 3).
581 We did not measure Zap70 expression in iNKT lineage cells. The decreased Zap70 expression in DP
582 thymocytes might contribute to the impaired positive selection and superantigen-mediated negative
583 selection of *PG* mice. It also could impact generation of the NKT2/17 cell population. Furthermore, it
584 could contribute to relative lack of fitness in of *PG* iNKT cells progressing from Stage 0 to Stage 1 when
585 competing with wild type cells. Independent of whether these Zap70 differences are causative of the
586 observed altered negative selection and NKT differentiation in *PG* mice, reduced Zap70 expression
587 demonstrates proof-of-concept that the Rag1^{P326G} mutation alters protein expression in developing αβ T

588 cells as suggested in our second hypothesis above. RAG DSBs induced in pre-B cells signal temporal
589 changes in gene transcription to modulate expression of proteins including transcription factors that
590 transcriptionally control expression of other proteins (23-25). Likewise, RAG DSBs generated in
591 lymphoid progenitor cells cause heritable changes in gene transcription that enhance the differentiation
592 and function of NK cells and other mature innate lymphoid cells (33). In normal mice, several rounds of
593 Vα-to-Jα rearrangement typically occur on each allele in a DP thymocytes until formation of an αβ TCR
594 that promotes positive selection (47). The decreased Vα-to-Jα rearrangements in DP thymocytes of *PG*
595 mice would correspond with fewer RAG DSBs to signal transcriptional changes in the expression of
596 proteins that govern selection and/or differentiation of αβ T lineage cells. One of these proteins could
597 enhance Zap70 protein expression, while another might promote NKT1 cell differentiation. Alternatively,
598 $Rag1^{P326G}$ mutation could prevent Rag1 from recruiting and/or ubiquitylating proteins that activate signals
599 from RAG DSBs to modulate the expression and/or activity of proteins including Zap70. We did not detect
600 differences in Zap70 activation or other aspects of TCR signaling between *WT* and *PG* thymocytes after
601 anti-CD3 stimulation (data not shown). However, this approach is not as sensitive for assaying signalling
602 differences as using tetramers or DCs to present peptides to transgenic αβ TCRs of fixed specificity (9,
603 48, 49)., which will be necessary to determine if $Rag1^{P326G}$ mutation diminishes TCR signaling in DP
604 thymocytes. A positive outcome would warrant determining the contribution of reduced Zap70 versus
605 other protein expression changes.
606
607 The requirement for TCR selection on self-peptides displayed by self-proteins presents major challenges
608 for establishing conventional and non-conventional αβ T cell populations that recognize and respond to a
609 vast array of diverse foreign peptides, but not self-antigens. Thus, cell intrinsic mechanisms have evolved
610 to render thymocytes more sensitive to TCR stimulation than their mature αβ T cell counterparts (48, 50-
611 53), a phenomenon called thymic TCR tuning (49, 54-58). Our data are consistent with the possibility that

612 the RAG1 RING domain ubiquitin ligase enhances thymic TCR tuning. Regardless, our study provides a
613 phenotypic framework from which to elucidate precise molecular mechanisms by which the RAG1 RING
614 domain regulates TCR gene assembly and selection to establish replete populations of αβ T lineage cells
615 and central tolerance.

616 **Materials and Methods**
617

618 **Mice**

619 C57BL/6 background *PG* mice were made through gene-targeting as performed by InGenious Targeting
620 Laboratory (2200 Smithtown Avenue, Ronkonkoma, NY). The 9.5 kb genomic DNA used to construct
621 the targeting vector was sub-cloned from a 129Svev BAC clone. The CC>GG double point mutation was
622 shuttled from pJMJ029[P326G](15) into the targeting vector using unique restriction sites, then confirmed
623 by sequencing. Linearized targeting vector was electroporated into BA1 (C57BL/6 x 129/SvEv)
624 embryonic stem (ES) cells. After selection with G418 antibiotic, clones were expanded for PCR analysis
625 to identify recombinant ES clones. Positive clones were screened for short arm integration and then
626 confirmation of the point mutation was performed by PCR and sequencing. Positive clones were analyzed
627 by Southern blot to confirm long arm integration. Injected blastocysts were grown in foster mothers and
628 chimeras were backcrossed against C57BL/6 mice to generate heterozygotes. These were crossed with
629 CMV-*cre* mice (JAX #006054)(60) to remove the *neo* reporter cassette and generate the $Rag1^{P326G}$ allele.
630 After confirmation of *neo* cassette removal, the strain was backcrossed against C57BL/6, and removal of
631 CMV-*cre* was confirmed by PCR. Sequencing of the entire *Rag1* locus in progeny confirmed the intended
632 CC>GG mutation and an additional T>C point mutation that generates a V238A substitution outside of
633 the RING finger domain. The strain was deposited at the Mutant Mouse Regional Resource Center at the
634 University of North Caroline (RAG1-tm1, MMRRC #: 37105). Before initiating studies described herein,
635 the $Rag1^{P326G}$ allele was backcrossed for nine generations onto the C57BL/6 background. C57BL/6
636 background wild-type and $Rag1^{-/-}$ mice and BALB/c background $Rag1^{-/-}$ mice were purchased from
637 Jackson Laboratories. All experimental mice were littermates or age-matched with control wild-type
638 animals. All experiments were conducted in accordance with national guidelines and approved by the
639 Institutional Animal Care and Use Committee (IACUC) of the Children's Hospital of Philadelphia.
640

641 **Flow Cytometry**

642 Single cell suspensions of all organs were ACK lysed to remove erythrocytes before being stained with
643 LIVE/DEAD™ Fixable Aqua Dead Cell Stain Kit (Invitrogen) and antibodies against respective surface
644 antigens (BD Biosciences, eBioscience, and Biolegend). Cells were stained for respective intracellular
645 proteins using Cytofix/Cytoperm Fixation/Permeabilization solution kit (BD Biosciences). For staining of
646 intracellular cytokines, cells (1 x10^6) were cultured in the absence or presence of 50 ng/ml PMA (Sigma)
647 and 1μg/ml Ionomycin (Cell Signaling Technology), with 2 μg/ml brefeldin A (Sigma) and 2 μM
648 monensin (eBioscience) for 4 hours at 37ºC. After staining for LIVE/DEAD and surface antigens, cells
649 were stained for respective cytokines using the Cytofix/Cytoperm kit (BD Bioscience) or transcription
650 factors using the FoxP3/Transcription Factor staining kit (eBiosciences). Data were acquired on a
651 MACSQuant flow cytometer (Miltenyi Biotec) or LSRII Fortessa (BD Biosciences) and analyzed using
652 Flowjo software version 10.5.3 (Tree Star). Analyses were conducted with the following antibodies: anti-
653 CD4 (APC-eFluor 780, clone RM4-5, 1:100), anti-CD25 (BUV395, clone PC61, 1:100), anti-TCRβ
654 (BV711, clone H57-597, 1:100), anti-CD19 (PE, clone 1D3, 1:100), anti-CD11b (PE, clone M1/70, 1:100),
655 anti-CD11c (PE, clone HL3, 1:100), anti-TER (PE, clone TER-119, 1:100), anti-TCRγ/δ (PE, clone GL3,
656 1:100), anti-NK-1.1 (PE, clone PK136, 1:100), and anti-B220 (PE, clone RA3-6B2, 1:100) from BD
657 Biosciences; or anti-CD8α (Pacific Blue, clone 53-6.7, 1:100), anti-CD44 (APC, PerCP/Cy5.5, clone IM7,
658 1:100), anti-CD24 (PE/Cy7, clone M1/69, 1:100), anti-CD28 (FITC, clone E18, 1:50), anti-CD45.1 (APC,
659 clone A20, 1:100), anti-C45.2 (FITC, clone 104, 1:100) from BioLegend.

660

661 **Cell Sorting**

662 To isolate DN3 cells, thymocytes were stained with PE-labelled CD4, CD8, CD11b, CD11c, NK1.1, Gr1,
663 and Ter119. Non-labelled cells were enriched by MACS depletion using anti-PE microbeads and LS
664 columns (Miltenyi). Enriched cells were then stained with CD4, CD8, CD44, CD25 and anti-lineage/stage
665 markers (TCRβ, B220, CD19, CD11b, CD11c, TCRδ, NK1.1, Ter119) antibodies. DN3 thymocytes were

666 sorted on Lin$^-$CD4$^-$CD8$^-$CD44$^-$CD25$^+$ phenotype. To isolate DP cells, thymocytes were stained with CD4,
667 CD8, and anti-lineage (B220, CD19, CD11b, CD11c, TCRδ, NK1.1, Ter119) antibodies. DP thymocytes
668 were sorted on Lin$^-$CD4$^+$CD8$^+$ phenotype. The cells of interest were isolated using a FACSAria Fusion
669 sorter (BD Biosciences).
670
671 **Analyzing *Tcrb* and *Tcra* Rearrangements**
672 Genomic DNA was extracted from DN3 or DP cells using the DNeasy Blood and Tissue kit (Qiagen). To
673 measure *Tcrb* rearrangements in DN3 cells, a Taqman PCR assay was used to quantify Vβ-to-DJβ1.1 and
674 Vβ-to-DJβ2.1 rearrangement levels with a primer specific for each Vβ paired and a probe, FAM or HEX,
675 specific for Jβ1.1 or Jβ2.1, respectively. Taqman PCR was performed with conditions according to the
676 manufacturer's instructions (IDT DNA) on the ViiA 7 system (Applied Biosystems). PCR of CD19 was
677 used for normalization. Primers, probes, and reaction conditions are as described (61). To assay *Tcrb*
678 repertoire, DNA from DN3 thymocytes were sent to Adaptive Biotechnologies, who used multiplex PCR
679 to amplify and deep sequence Vβ-Dβ-Jβ rearrangements. Gene segment usage was analyzed by
680 ImmunoSEQ Analyzer software (Adaptive Biotechnologies). To assess *Tcra* rearrangements in DP cells,
681 representative Vα-Jα rearrangements were quantified using a QuantiFast SYBR Green PCR kit (Qiagen)
682 on the ViiA 7 system (Applied Biosystems) as described (62, 63). PCR of β2M was used for normalization.
683 We quantified Vα14-Jα18 rearrangments as described (64).
684
685 **RT-qPCR for mRNA Expression**
686 Respective cell populations were lysed in RLT buffer (Qiagen) containing 2-mercaptoethanol or TRIzol
687 (Life Technologies) immediately after cell sorting. Total RNA was isolated using RNeasy Mini kit
688 (Qiagen), treated with DNase (RNase-Free DNase Set, Qiagen), and reverse transcribed to generate cDNA
689 with High-Capacity RNA-to-cDNA™ Kit (Themo-Fisher Scientific) according to manufacturer's

690 directions. The cDNA was subjected to qPCR using Power SYBR Green kit (Applied Biosystems) and
691 actin, HPRT, ZAP70, and SYK primers (Qiagen). Relative expression was calculated using the ddCt
692 method, using actin or HPRT as a housekeeping gene, and relevant calibrator sample (explained in figure
693 legends for respective samples).
694
695 **Competitive Mixed Bone Marrow Chimeric Mice**
696 6-week-old CD45.1 B6.SJL (WT) hosts were lethally irradiated (950 Rad on an X-RAD irradiator). Bone
697 marrow from at least 3 pooled donors (CD45.1 WT only, CD45.2 RAG P326G mutant only, or mixed)
698 was sterilely prepped and RBCs lysed. Acceptable mixing (CD45.1/CD45.2 ratio) was confirmed by flow
699 cytometry. Then, 3-5x10^6 total cells were injected intravenously into hosts 6 hours after irradiation. Mice
700 were monitored over 8 weeks for graft rejection and graft-versus-host disease prior to euthanasia for
701 analysis. Engraftment was measured using the following antibodies from Biolegend: anti-CD45.1 (APC-
702 Cy7, clone A20, 1:100), anti-CD45.2 (FITC, Clone 104, 1:100), anti-NK1.1 (PE, clone PK136, 1:200),
703 anti-CD44 (PerCP-Cy5.5, clone IM7, 1:100), anti CD24 (PE-Cy7, clone M1/69, 1:100), and anti-TCRβ
704 (Pacific blue, clone H57-597, 1:100). CD1d tetramer from the NIH Tetramer Core (APC, 1:100) was a
705 gift of Dr. Hamid Bassiri. Data were collected on a MACSQuant 10 (Miltenyi Biotec) and were analyzed
706 using FlowJo software, version 10.
707
708 ***In vitro* T Cell Differentiation**
709 Splenocytes from C57BL/6 background *Rag1*$^{-/-}$ mice were irradiated with 2,500 Rads (X-rad irradiator)
710 and 3 x 10^5 cells were seeded into each well of a 96 well plate. Naïve T cells (CD90.2$^+$, CD4$^+$, CD62L$^+$,
711 CD44$^+$, CD25$^-$) were sorted from C57BL/6 background *WT* or *Rag1*$^{-/-}$ mice using a FACSaria Fusion cell
712 sorter (BD Biosciences), and 3 x 10^4 sorted cells were added to each well containing irradiated feeder
713 cells. All cells were cultured with 10 μg/ml anti-CD3 (Biolegend) and 3 μg/ml anti-CD28 (Biolegend) in
714 RPMI with 10% FBS, 1% PSG, and 1x NEAA (Invitrogen), 1x Sodium Pyruvate (Invitrogen), and 0.001%

715 2-mercaptoethanol. rhIL-2 was used at 30 IU/mL, rmIL-12 and rmIL-4 at 10 ng/mL, rmIL-6 at 20 ng/mL,
716 mTGFβ1 at 1 ng/mL, anti-mIL-4, anti-mIFNγ and anti-mIL-12 at 10 μg/mL (from Biolegend except rhIL-
717 2, rmIL-12, and rmIL-6 from Prepotech). The following cytokines/blocking antibodies were used to skew
718 towards respective Th-subsets: Th0 condition: rhIL-2; Th1 condition: rhIL-2, rmIL-12 and anti-mIL-4;
719 Th2 condition: rhIL-2, rmIL-4, anti-mIFNγ and anti-mIL-12; Th17 condition: rhIL-2, mIL-6, mTGFβ1,
720 anti-mIL-4 and anti-mIL-12; Treg condition: rhIL-2, mTGFβ1, anti-mIL-4 and anti-mIL-12.
721

722 **LCMV Infections**

723 Mice were infected intraperitoneally with 2 x 10^5 plaque-forming units of LCMV-Armstrong and
724 euthanized at indicated timepoints. Virus and gp33-tetramer were kindly provided by E. John Wherry
725 (University of Pennsylvania).
726

727 **T Cell Transfer Model of Colitis**

728 This model was performed as described (37). Briefly, naïve $CD4^+$ T cells were sorted from respective
729 donor mice ($CD90.2^+$, $CD4^+$, $CD62L^+$, $CD44^-$, $CD25^-$) on a FACSAria Fusion cell sorter. 0.5 x 10^6 cells
730 were transferred in 100 μl of PBS into each of the donor mice via intraperitoneal injection. Non-transferred
731 mice were injected with PBS. Mice were weighed weekly for the first 4 weeks, and then twice weekly for
732 4 weeks. Mice were euthanized 8 weeks post-transfer unless severe morbidity enforced premature
733 euthanasia (in accordance with CHOP IACUC approved guidelines) or spontaneous death occurred.
734

735 **Statistical analysis**

736 All data was analyzed in Graphpad Prism 8 using statistical tests indicated in the figure legends. Error
737 bars indicate mean +/- SEM unless otherwise stated. n.s.=$p>0.05$, *$p<0.05$, **$p<0.01$, ***$p<0.001$,
738 ****$p<0.0001$.

Acknowledgements

The authors have no competing financial interests to declare.

741 **References**
742

743 1. Bassing, C. H., W. Swat, and F. W. Alt. 2002. The mechanism and regulation of chromosomal
744 V(D)J recombination. *Cell* 109 Suppl: S45-55.
745 2. Schatz, D. G., and P. C. Swanson. 2011. V(D)J recombination: mechanisms of initiation. *Annu*
746 *Rev Genet* 45: 167-202.
747 3. Bhandoola, A., H. von Boehmer, H. T. Petrie, and J. C. Zuniga-Pflucker. 2007. Commitment and
748 developmental potential of extrathymic and intrathymic T cell precursors: plenty to choose from.
749 *Immunity* 26: 678-689.
750 4. von Boehmer, H., and F. Melchers. 2010. Checkpoints in lymphocyte development and
751 autoimmune disease. *Nat Immunol* 11: 14-20.
752 5. Carico, Z., and M. S. Krangel. 2015. Chromatin Dynamics and the Development of the TCRalpha
753 and TCRdelta Repertoires. *Adv Immunol* 128: 307-361.
754 6. Hogquist, K. A., and S. C. Jameson. 2014. The self-obsession of T cells: how TCR signaling
755 thresholds affect fate 'decisions' and effector function. *Nat Immunol* 15: 815-823.
756 7. Gascoigne, N. R., V. Rybakin, O. Acuto, and J. Brzostek. 2016. TCR Signal Strength and T Cell
757 Development. *Annu Rev Cell Dev Biol* 32: 327-348.
758 8. Klein, L., B. Kyewski, P. M. Allen, and K. A. Hogquist. 2014. Positive and negative selection of
759 the T cell repertoire: what thymocytes see (and don't see). *Nat Rev Immunol* 14: 377-391.
760 9. Fu, G., V. Rybakin, J. Brzostek, W. Paster, O. Acuto, and N. R. Gascoigne. 2014. Fine-tuning T
761 cell receptor signaling to control T cell development. *Trends Immunol* 35: 311-318.
762 10. Jones, J. M., and M. Gellert. 2003. Autoubiquitylation of the V(D)J recombinase protein RAG1.
763 *Proc Natl Acad Sci U S A* 100: 15446-15451.
764 11. Singh, S. K., and M. Gellert. 2015. Role of RAG1 autoubiquitination in V(D)J recombination.
765 *Proc Natl Acad Sci U S A* 112: 8579-8583.
766 12. Jones, J. M., A. Bhattacharyya, C. Simkus, B. Vallieres, T. D. Veenstra, and M. Zhou. 2011. The
767 RAG1 V(D)J recombinase/ubiquitin ligase promotes ubiquitylation of acetylated, phosphorylated
768 histone 3.3. *Immunol Lett* 136: 156-162.
769 13. Grazini, U., F. Zanardi, E. Citterio, S. Casola, C. R. Goding, and F. McBlane. 2010. The RING
770 domain of RAG1 ubiquitylates histone H3: a novel activity in chromatin-mediated regulation of
771 V(D)J joining. *Mol Cell* 37: 282-293.
772 14. Deng, Z., H. Liu, and X. Liu. 2015. RAG1-mediated ubiquitylation of histone H3 is required for
773 chromosomal V(D)J recombination. *Cell Res* 25: 181-192.
774 15. Simkus, C., P. Anand, A. Bhattacharyya, and J. M. Jones. 2007. Biochemical and folding defects
775 in a RAG1 variant associated with Omenn syndrome. *J Immunol* 179: 8332-8340.
776 16. Villa, A., C. Sobacchi, L. D. Notarangelo, F. Bozzi, M. Abinun, T. G. Abrahamsen, P. D.
777 Arkwright, M. Baniyash, E. G. Brooks, M. E. Conley, P. Cortes, M. Duse, A. Fasth, A. M.
778 Filipovich, A. J. Infante, A. Jones, E. Mazzolari, S. M. Muller, S. Pasic, G. Rechavi, M. G. Sacco,
779 S. Santagata, M. L. Schroeder, R. Seger, D. Strina, A. Ugazio, J. Valiaho, M. Vihinen, L. B. Vogler,
780 H. Ochs, P. Vezzoni, W. Friedrich, and K. Schwarz. 2001. V(D)J recombination defects in
781 lymphocytes due to RAG mutations: severe immunodeficiency with a spectrum of clinical
782 presentations. *Blood* 97: 81-88.
783 17. Zheng, N., P. Wang, P. D. Jeffrey, and N. P. Pavletich. 2000. Structure of a c-Cbl-UbcH7 complex:
784 RING domain function in ubiquitin-protein ligases. *Cell* 102: 533-539.
785 18. Albert, T. K., H. Hanzawa, Y. I. Legtenberg, M. J. de Ruwe, F. A. van den Heuvel, M. A. Collart,
786 R. Boelens, and H. T. Timmers. 2002. Identification of a ubiquitin-protein ligase subunit within
787 the CCR4-NOT transcription repressor complex. *EMBO J* 21: 355-364.
788 19. Beilinson, H. A., R. A. Glynn, A. D. Yadavalli, J. Xiao, E. Corbett, H. Saribasak, R. Arya, C. Miot,
789 A. Bhattacharyya, J. M. Jones, J. M. R. Pongubala, C. H. Bassing, and D. G. Schatz. 2021. The

790 RAG1 N-terminal region regulates the efficiency and pathways of synapsis for V(D)J
791 recombination. *J Exp Med* 218.
792 20. Liang, H. E., L. Y. Hsu, D. Cado, L. G. Cowell, G. Kelsoe, and M. S. Schlissel. 2002. The
793 "dispensable" portion of RAG2 is necessary for efficient V-to-DJ rearrangement during B and T
794 cell development. *Immunity* 17: 639-651.
795 21. Horowitz, J. E., and C. H. Bassing. 2014. Noncore RAG1 regions promote Vbeta rearrangements
796 and alphabeta T cell development by overcoming inherent inefficiency of Vbeta recombination
797 signal sequences. *J Immunol* 192: 1609-1619.
798 22. Williams, J. A., K. S. Hathcock, D. Klug, Y. Harada, B. Choudhury, J. P. Allison, R. Abe, and R.
799 J. Hodes. 2005. Regulated costimulation in the thymus is critical for T cell development:
800 dysregulated CD28 costimulation can bypass the pre-TCR checkpoint. *J Immunol* 175: 4199-4207.
801 23. Bredemeyer, A. L., B. A. Helmink, C. L. Innes, B. Calderon, L. M. McGinnis, G. K. Mahowald,
802 E. J. Gapud, L. M. Walker, J. B. Collins, B. K. Weaver, L. Mandik-Nayak, R. D. Schreiber, P. M.
803 Allen, M. J. May, R. S. Paules, C. H. Bassing, and B. P. Sleckman. 2008. DNA double-strand
804 breaks activate a multi-functional genetic program in developing lymphocytes. *Nature* 456: 819-
805 823.
806 24. Bednarski, J. J., A. Nickless, D. Bhattacharya, R. H. Amin, M. S. Schlissel, and B. P. Sleckman.
807 2012. RAG-induced DNA double-strand breaks signal through Pim2 to promote pre-B cell
808 survival and limit proliferation. *J Exp Med* 209: 11-17.
809 25. Bednarski, J. J., R. Pandey, E. Schulte, L. S. White, B. R. Chen, G. J. Sandoval, M. Kohyama, M.
810 Haldar, A. Nickless, A. Trott, G. Cheng, K. M. Murphy, C. H. Bassing, J. E. Payton, and B. P.
811 Sleckman. 2016. RAG-mediated DNA double-strand breaks activate a cell type-specific
812 checkpoint to inhibit pre-B cell receptor signals. *J Exp Med* 213: 209-223.
813 26. Jordan, M. S., J. E. Smith, J. C. Burns, J. E. Austin, K. E. Nichols, A. C. Aschenbrenner, and G.
814 A. Koretzky. 2008. Complementation in trans of altered thymocyte development in mice
815 expressing mutant forms of the adaptor molecule SLP76. *Immunity* 28: 359-369.
816 27. Surh, C. D., and J. Sprent. 1994. T-cell apoptosis detected in situ during positive and negative
817 selection in the thymus. *Nature* 372: 100-103.
818 28. Wilson, A., C. Marechal, and H. R. MacDonald. 2001. Biased V beta usage in immature
819 thymocytes is independent of DJ beta proximity and pT alpha pairing. *J Immunol* 166: 51-57.
820 29. Rossjohn, J., D. G. Pellicci, O. Patel, L. Gapin, and D. I. Godfrey. 2012. Recognition of CD1d-
821 restricted antigens by natural killer T cells. *Nat Rev Immunol* 12: 845-857.
822 30. Krovi, S. H., and L. Gapin. 2018. Invariant Natural Killer T Cell Subsets-More Than Just
823 Developmental Intermediates. *Front Immunol* 9: 1393.
824 31. Dashtsoodol, N., S. Bortoluzzi, and M. Schmidt-Supprian. 2019. T Cell Receptor Expression
825 Timing and Signal Strength in the Functional Differentiation of Invariant Natural Killer T Cells.
826 *Front Immunol* 10: 841.
827 32. Hogquist, K., and H. Georgiev. 2020. Recent advances in iNKT cell development. *F1000Res* 9.
828 33. Karo, J. M., D. G. Schatz, and J. C. Sun. 2014. The RAG recombinase dictates functional
829 heterogeneity and cellular fitness in natural killer cells. *Cell* 159: 94-107.
830 34. Jiang, W., M. S. Anderson, R. Bronson, D. Mathis, and C. Benoist. 2005. Modifier loci condition
831 autoimmunity provoked by Aire deficiency. *J Exp Med* 202: 805-815.
832 35. Jin, Y., A. Lee, J. H. Oh, H. W. Lee, and S. J. Ha. 2019. The R229Q mutation of Rag2 does not
833 characterize severe immunodeficiency in mice. *Sci Rep* 9: 4415.
834 36. Mottet, C., H. H. Uhlig, and F. Powrie. 2003. Cutting edge: cure of colitis by CD4+CD25+
835 regulatory T cells. *J Immunol* 170: 3939-3943.
836 37. Ostanin, D. V., J. Bao, I. Koboziev, L. Gray, S. A. Robinson-Jackson, M. Kosloski-Davidson, V.
837 H. Price, and M. B. Grisham. 2009. T cell transfer model of chronic colitis: concepts,
838 considerations, and tricks of the trade. *Am J Physiol Gastrointest Liver Physiol* 296: G135-146.

839 38. Eri, R., M. A. McGuckin, and R. Wadley. 2012. T cell transfer model of colitis: a great tool to
840 assess the contribution of T cells in chronic intestinal inflammation. *Methods Mol Biol* 844: 261-
841 275.
842 39. Livak, F., D. B. Burtrum, L. Rowen, D. G. Schatz, and H. T. Petrie. 2000. Genetic modulation of
843 T cell receptor gene segment usage during somatic recombination. *J Exp Med* 192: 1191-1196.
844 40. Bortoluzzi, S., N. Dashtsoodol, T. Engleitner, C. Drees, S. Helmrath, J. Mir, A. Toska, M.
845 Flossdorf, R. Ollinger, M. Solovey, M. Colome-Tatche, B. Kalfaoglu, M. Ono, T. Buch, T.
846 Ammon, R. Rad, and M. Schmidt-Supprian. 2021. Brief homogeneous TCR signals instruct
847 common iNKT progenitors whose effector diversification is characterized by subsequent cytokine
848 signaling. *Immunity* 54: 2497-2513 e2499.
849 41. Cameron, G., D. G. Pellicci, A. P. Uldrich, G. S. Besra, P. Illarionov, S. J. Williams, N. L. La
850 Gruta, J. Rossjohn, and D. I. Godfrey. 2015. Antigen Specificity of Type I NKT Cells Is Governed
851 by TCR beta-Chain Diversity. *J Immunol* 195: 4604-4614.
852 42. Negishi, I., N. Motoyama, K. Nakayama, K. Nakayama, S. Senju, S. Hatakeyama, Q. Zhang, A.
853 C. Chan, and D. Y. Loh. 1995. Essential role for ZAP-70 in both positive and negative selection
854 of thymocytes. *Nature* 376: 435-438.
855 43. Hsu, L. Y., Y. X. Tan, Z. Xiao, M. Malissen, and A. Weiss. 2009. A hypomorphic allele of ZAP-
856 70 reveals a distinct thymic threshold for autoimmune disease versus autoimmune reactivity. *J Exp*
857 *Med* 206: 2527-2541.
858 44. Sakaguchi, N., T. Takahashi, H. Hata, T. Nomura, T. Tagami, S. Yamazaki, T. Sakihama, T.
859 Matsutani, I. Negishi, S. Nakatsuru, and S. Sakaguchi. 2003. Altered thymic T-cell selection due
860 to a mutation of the ZAP-70 gene causes autoimmune arthritis in mice. *Nature* 426: 454-460.
861 45. Zhao, M., M. N. D. Svensson, K. Venken, A. Chawla, S. Liang, I. Engel, P. Mydel, J. Day, D.
862 Elewaut, N. Bottini, and M. Kronenberg. 2018. Altered thymic differentiation and modulation of
863 arthritis by invariant NKT cells expressing mutant ZAP70. *Nat Commun* 9: 2627.
864 46. Tuttle, K. D., S. H. Krovi, J. Zhang, R. Bedel, L. Harmacek, L. K. Peterson, L. L. Dragone, A.
865 Lefferts, C. Halluszczak, K. Riemondy, J. R. Hesselberth, A. Rao, B. P. O'Connor, P. Marrack, J.
866 Scott-Browne, and L. Gapin. 2018. TCR signal strength controls thymic differentiation of iNKT
867 cell subsets. *Nat Commun* 9: 2650.
868 47. Huang, C. Y., B. P. Sleckman, and O. Kanagawa. 2005. Revision of T cell receptor {alpha} chain
869 genes is required for normal T lymphocyte development. *Proc Natl Acad Sci U S A* 102: 14356-
870 14361.
871 48. Davey, G. M., S. L. Schober, B. T. Endrizzi, A. K. Dutcher, S. C. Jameson, and K. A. Hogquist.
872 1998. Preselection thymocytes are more sensitive to T cell receptor stimulation than mature T cells.
873 *J Exp Med* 188: 1867-1874.
874 49. Fu, G., J. Casas, S. Rigaud, V. Rybakin, F. Lambolez, J. Brzostek, J. A. Hoerter, W. Paster, O.
875 Acuto, H. Cheroutre, K. Sauer, and N. R. Gascoigne. 2013. Themis sets the signal threshold for
876 positive and negative selection in T-cell development. *Nature* 504: 441-445.
877 50. Lucas, B., I. Stefanova, K. Yasutomo, N. Dautigny, and R. N. Germain. 1999. Divergent changes
878 in the sensitivity of maturing T cells to structurally related ligands underlies formation of a useful
879 T cell repertoire. *Immunity* 10: 367-376.
880 51. Yachi, P. P., C. Lotz, J. Ampudia, and N. R. Gascoigne. 2007. T cell activation enhancement by
881 endogenous pMHC acts for both weak and strong agonists but varies with differentiation state. *J*
882 *Exp Med* 204: 2747-2757.
883 52. Pircher, H., U. H. Rohrer, D. Moskophidis, R. M. Zinkernagel, and H. Hengartner. 1991. Lower
884 receptor avidity required for thymic clonal deletion than for effector T-cell function. *Nature* 351:
885 482-485.
886 53. Sant'Angelo, D. B., and C. A. Janeway, Jr. 2002. Negative selection of thymocytes expressing the
887 D10 TCR. *Proc Natl Acad Sci U S A* 99: 6931-6936.

54. Fu, G., S. Vallee, V. Rybakin, M. V. McGuire, J. Ampudia, C. Brockmeyer, M. Salek, P. R. Fallen, J. A. Hoerter, A. Munshi, Y. H. Huang, J. Hu, H. S. Fox, K. Sauer, O. Acuto, and N. R. Gascoigne. 2009. Themis controls thymocyte selection through regulation of T cell antigen receptor-mediated signaling. *Nat Immunol* 10: 848-856.
55. Lesourne, R., S. Uehara, J. Lee, K. D. Song, L. Li, J. Pinkhasov, Y. Zhang, N. P. Weng, K. F. Wildt, L. Wang, R. Bosselut, and P. E. Love. 2009. Themis, a T cell-specific protein important for late thymocyte development. *Nat Immunol* 10: 840-847.
56. Johnson, A. L., L. Aravind, N. Shulzhenko, A. Morgun, S. Y. Choi, T. L. Crockford, T. Lambe, H. Domaschenz, E. M. Kucharska, L. Zheng, C. G. Vinuesa, M. J. Lenardo, C. C. Goodnow, R. J. Cornall, and R. H. Schwartz. 2009. Themis is a member of a new metazoan gene family and is required for the completion of thymocyte positive selection. *Nat Immunol* 10: 831-839.
57. Wang, D., M. Zheng, L. Lei, J. Ji, Y. Yao, Y. Qiu, L. Ma, J. Lou, C. Ouyang, X. Zhang, Y. He, J. Chi, L. Wang, Y. Kuang, J. Wang, X. Cao, and L. Lu. 2012. Tespa1 is involved in late thymocyte development through the regulation of TCR-mediated signaling. *Nat Immunol* 13: 560-568.
58. Li, Q. J., J. Chau, P. J. Ebert, G. Sylvester, H. Min, G. Liu, R. Braich, M. Manoharan, J. Soutschek, P. Skare, L. O. Klein, M. M. Davis, and C. Z. Chen. 2007. miR-181a is an intrinsic modulator of T cell sensitivity and selection. *Cell* 129: 147-161.
59. Marrella, V., P. L. Poliani, A. Casati, F. Rucci, L. Frascoli, M. L. Gougeon, B. Lemercier, M. Bosticardo, M. Ravanini, M. Battaglia, M. G. Roncarolo, M. Cavazzana-Calvo, F. Facchetti, L. D. Notarangelo, P. Vezzoni, F. Grassi, and A. Villa. 2007. A hypomorphic R229Q Rag2 mouse mutant recapitulates human Omenn syndrome. *J Clin Invest* 117: 1260-1269.
60. Schwenk, F., U. Baron, and K. Rajewsky. 1995. A cre-transgenic mouse strain for the ubiquitous deletion of loxP-flanked gene segments including deletion in germ cells. *Nucleic Acids Res* 23: 5080-5081.
61. Gopalakrishnan, S., K. Majumder, A. Predeus, Y. Huang, O. I. Koues, J. Verma-Gaur, S. Loguercio, A. I. Su, A. J. Feeney, M. N. Artyomov, and E. M. Oltz. 2013. Unifying model for molecular determinants of the preselection Vbeta repertoire. *Proc Natl Acad Sci U S A* 110: E3206-3215.
62. Shih, H. Y., J. Verma-Gaur, A. Torkamani, A. J. Feeney, N. Galjart, and M. S. Krangel. 2012. Tcra gene recombination is supported by a Tcra enhancer- and CTCF-dependent chromatin hub. *Proc Natl Acad Sci U S A* 109: E3493-3502.
63. Chen, L., Z. Carico, H. Y. Shih, and M. S. Krangel. 2015. A discrete chromatin loop in the mouse Tcra-Tcrd locus shapes the TCRdelta and TCRalpha repertoires. *Nat Immunol* 16: 1085-1093.
64. Gapin, L., J. L. Matsuda, C. D. Surh, and M. Kronenberg. 2001. NKT cells derive from double-positive thymocytes that are positively selected by CD1d. *Nat Immunol* 2: 971-978.

932 **Footnotes**

933 This work was supported by the Fondation ARC pour la recherche sur le cancer (C.M.), La Ligue contre
934 le cancer (C.M.), Fondation Pasteur Mutualite (C.M.), Nancy Taylor Foundation for Chronic Disease
935 (E.M.B.) and NIH grants R03 AI097611 (J.M.J.), R01 HL112836 (E.M.B.), R01 AI121250-A1
936 (E.M.B.), R21 A1 135435 (C.H.B.), and RO1 AI 112621 (C.H.B.).
937

938 **Supplemental Figures**

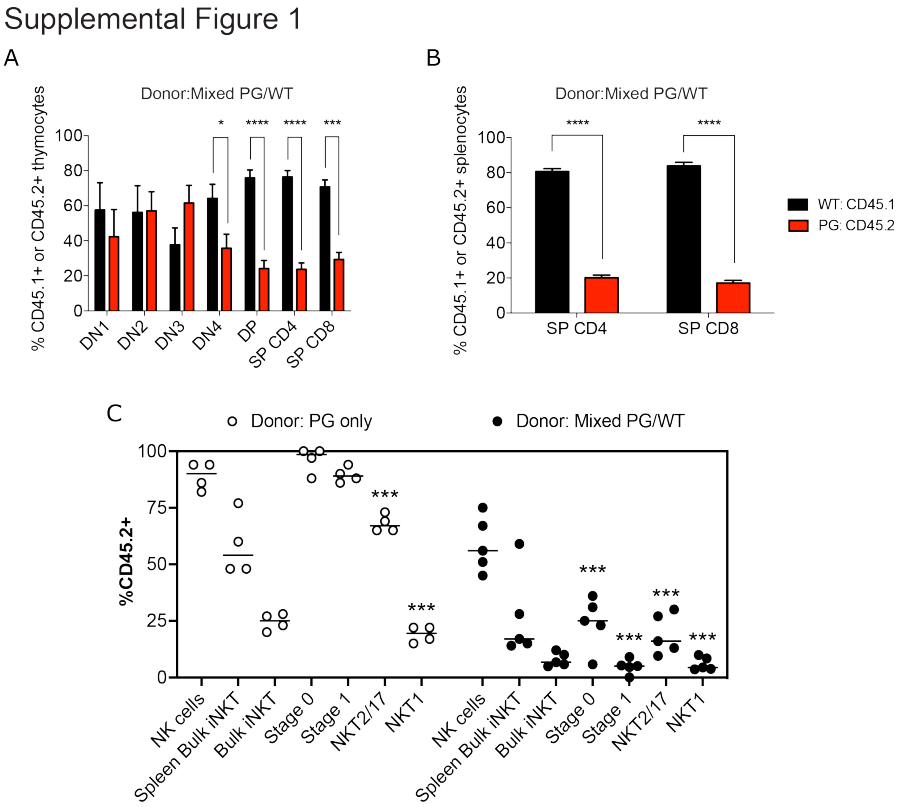

939

940 **Supplemental Figure 1.** *PG* thymocytes exhibit cell intrinsic deficiencies in developmental progression.

941 **(A-B)** Shown are percent of donor *PG* (CD45.2$^+$) or *WT* (CD45.1$^+$) cells within indicated (A) thymocyte

942 or (B) splenocyte populations after transfer of a 1:1 mix of *PG* and *WT* bone marrow into lethally irradiated

943 *WT* congenic (CD45.1$^+$) recipients. Bone marrow was pooled from three donors of each genotype and

944 injected into five recipients, all analyzed on the same day. Data represented as mean +/- SEM. Statistics

945 calculated with multiple t tests using the Holm-Sidak method. *p<0.05, ***p<0.0005, ****p<0.00005.

946 **(C)** Shown are percent donor *PG* (CD45.2$^+$) chimerism in indicated compartments after lethal irradiation

947 of *WT* congenic (CD45.1$^+$) recipients. Open circles show percent *PG* chimerism after transfer of only *PG*

948 bone marrow, while filled circles show *PG* chimerism in a 1:1 competitive setting with *WT* cells. *PG*

949 bone marrow reconstitutes the blood NK cell compartment at expected ratios. In mice receiving only *PG*

950 bone marrow, *PG* chimerism in bulk splenic iNKT (p<0.0001), bulk thymic iNKT (p<0.0001), NKT2/17

951 (p=0.001), and NKT1 (p<0.0001) are all significantly reduced relative to blood NK cells by one-way

952 ANOVA with Dunnett multiple comparisons test. In mice receiving 1:1 mixed *PG* and *WT* bone marrow,

953 *PG* chimerism in bulk splenic iNKT ($p=0.0002$), bulk thymic iNKT ($p<0.0001$), Stage 0 iNKT ($p<0.0001$),
954 Stage 1 iNKT ($p<0.0001$), Stage 2 iNKT ($p=0.001$), and Stage 3 iNKT ($p<0.0001$) are all significantly
955 reduced relative to blood NK cells. Bone marrow was pooled from three donors and injected into 4-5
956 mice per group, all analyzed on the same day.
957
958
959
960
961
962
963
964
965
966
967
968
969
970

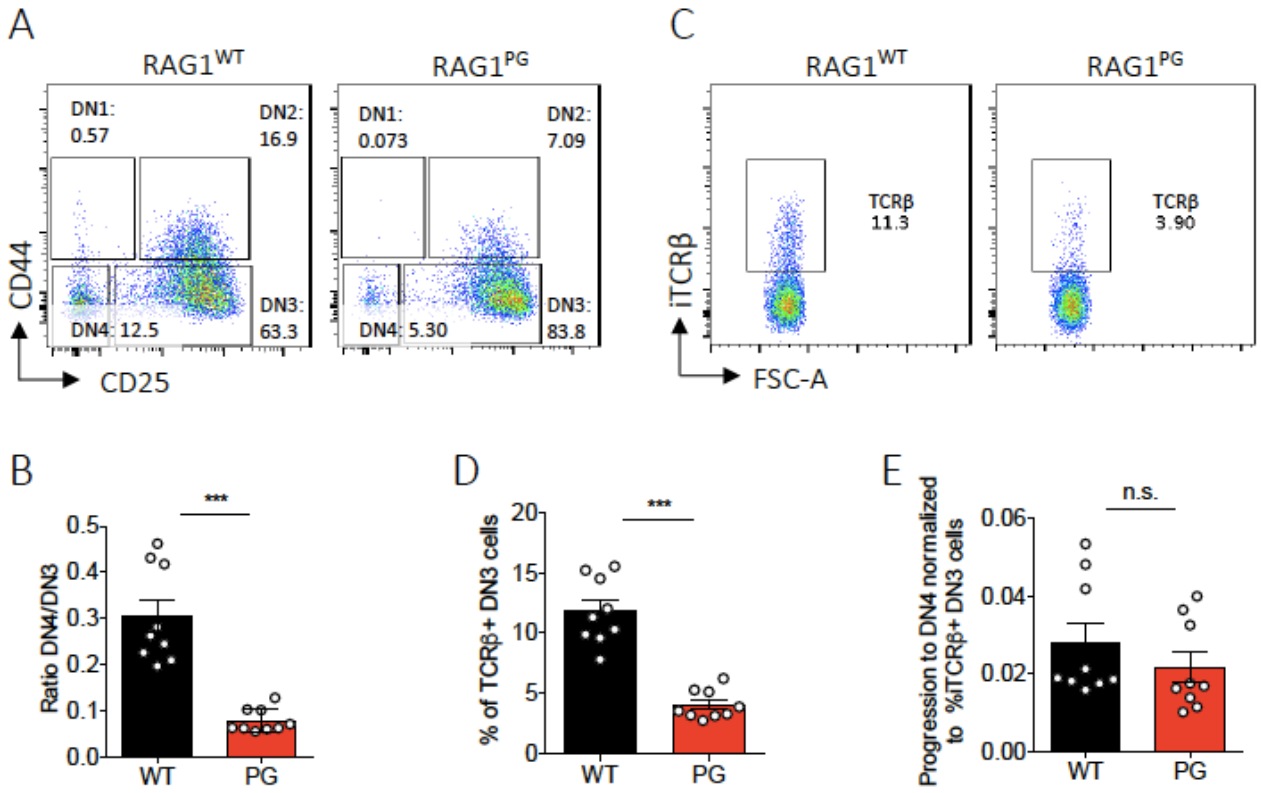

Supplemental Figure 2. *PG* mice exhibit normal efficiency of pre-TCR signaled DN3-to-DN4 thymocyte differentiation. **(A)** Representative flow cytometry plots of DN stages of thymocyte development showing the frequency of cells at the DN3 and DN4 stages. **(B)** Quantification of percentages of DN3 cells that transition into DN4 cells. Shown are all data points and average values +/- SEM from three independent experiments, each with three mice of each genotype (n = 9 mice per genotype, analyzed by multiple t tests using the Holm-Sidak method; *** $p<0.0005$). **(C)** Representative flow cytometry plots of intracellular TCRβ protein expression in DN3 thymocytes showing the frequency of TCRβ$^+$ cells in each gate. **(D)** Quantification of percentages of DN3 cells expressing intracellular TCRβ protein. **(E)** Ratios comparing the percentages of DN3 cells expressing intracellular TCRβ protein to the percentages of DN3 cells that transition into DN4 cells. (D-E) Shown are all data points and average values +/- SEM from three independent experiments each with three mice of each genotype (n = 9 mice per genotype, analyzed by unpaired t-test with Welch's correction; n.s. $p>0.05$, *** $p<0.0005$

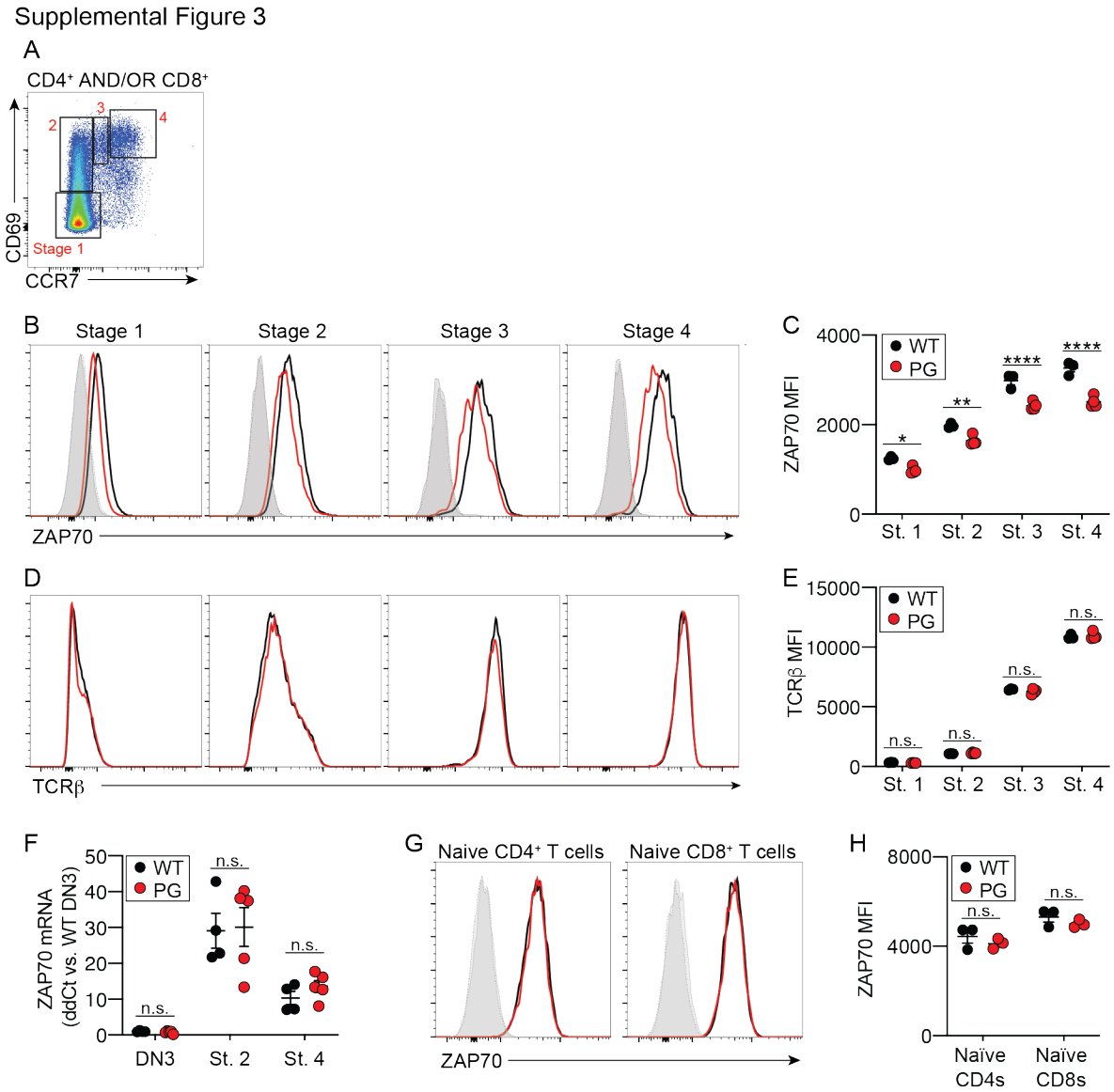

Supplemental Figure 3.

Thymocytes of PD mice have reduced Zap70 protein levels **(A)** Example gating strategy for Stage 1 - Stage 4 selecting thymocytes as depicted in Figure 4 and 5. Pre-gating: Live, singlets, $CD4^+$ AND/OR $CD8^+$. Stage 1 = $CD69^-CCR7^-$, Stage 2 = $CD69^+CCR7^-$, Stage 3 = $CD69^+CCR7^{int}$, Stage 4 = $CD69^+CCR7^{hi}$. **(B-E)** Representative flow cytometry histogram plots (B, D) and quantification (C, E) of Zap70 (B, C) and TCRβ (D, E) protein in Stages 1-4 of αβ TCR selection. (C, E) Shown are all data points and average values +/- SEM from one of three independent experiments (n = 4-5 mice per genotype, 2-way ANOVA with Sidak's multiple comparison post-test) **(F)** qRT-PCR quantification of Zap70 mRNA

993 in DN3 cells or Stage 2 or 4 cells. Relative mRNA levels were calculated using ddCt method with signals
994 from each assay normalized to values from an assay for the Hprt gene. Shown are all data points and
995 average values +/- SEM from one experiment (n = 4-5 mice per genotype, 2-way ANOVA with sidak
996 multiple comparison post-test. **(G-H)** Representative flow cytometry histogram plots (G) and
997 quantification (H) of Zap70 protein in naïve $CD4^+$ or $CD8^+$ T cells. Shown are all data points and average
998 values +/- SEM from two independent experiments (n = 3 mice per genotype, 2-way ANOVA with Sidak
999 multiple comparison post-test). For all graphs in figure: n.s. $p>0.05$; * $p<0.05$, ** $p<0.01$, *** $p<0.001$,
1000 **** $p<0.0001$.
1001